Article

Cell Reports

Vectorial Import via a Metastable Disulfide-Linked Complex Allows for a Quality Control Step and Import by the Mitochondrial Disulfide Relay

Graphical Abstract

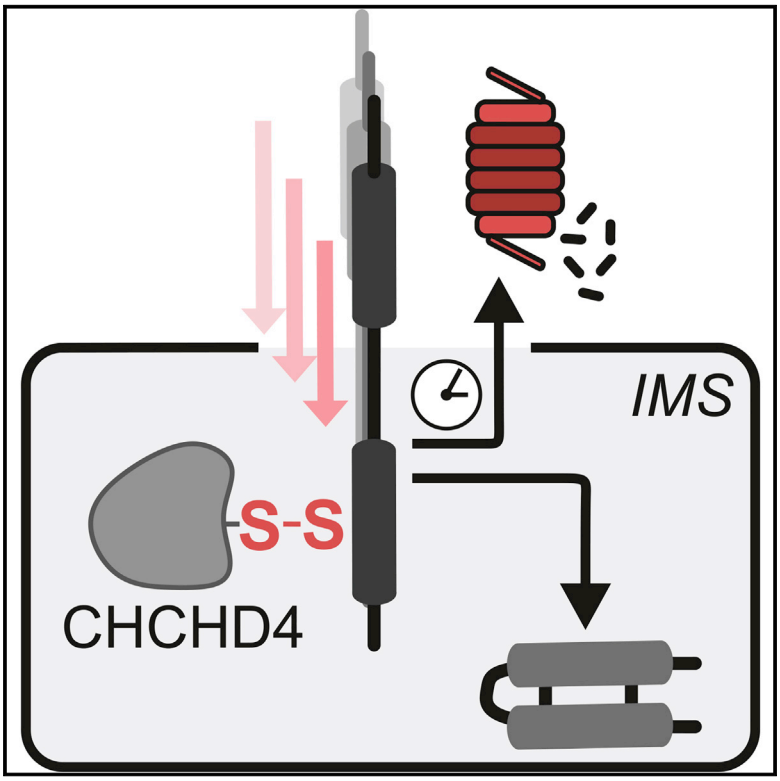

Authors

Markus Habich, Silja Lucia Salscheider, Lena Maria Murschall, ..., Hamid Kashkar, Joern Dengjel, Jan Riemer

Correspondence

jan.riemer@uni-koeln.de

In Brief

Disulfide formation in the mitochondrial intermembrane space (IMS) is an essential process that is coupled to protein import. Here, Habich et al. report on a redox quality control step in which the import competence of substrates is tested, and when it fails, substrates are released to the cytosol for degradation.

Highlights

- IMS import by the disulfide relay proceeds via formation of a covalent intermediate
- Import is driven by hydrophobic and disulfide-dependent interactions
- The covalent intermediate is also formed by oxidation-incompetent substrates
- Redox quality control allows for IMS substrate release and proteasomal degradation

Habich et al., 2019, Cell Reports *26*, 759–774
January 15, 2019
https://doi.org/10.1016/j.celrep.2018.12.092

CellPress

Cell Reports
Article

Vectorial Import via a Metastable Disulfide-Linked Complex Allows for a Quality Control Step and Import by the Mitochondrial Disulfide Relay

Markus Habich,[1] Silja Lucia Salscheider,[1] Lena Maria Murschall,[1] Michaela Nicole Hoehne,[1] Manuel Fischer,[1] Fabian Schorn,[2] Carmelina Petrungaro,[1] Muna Ali,[1] Alican J. Erdogan,[1] Shadi Abou-Eid,[3] Hamid Kashkar,[2] Joern Dengjel,[3] and Jan Riemer[1,4,*]

[1]Institute for Biochemistry, Department of Chemistry, University of Cologne, Zuelpicher Str. 47a/R. 3.49, 50674 Cologne, Germany
[2]Cologne Excellence Cluster on Cellular Stress Responses in Aging-Associated Diseases (CECAD), Center for Molecular Medicine Cologne (CMMC) and Institute for Medical Microbiology, Immunology and Hygiene, University of Cologne, CECAD Research Center, Joseph-Stelzmann-Str. 26, 50931 Cologne, Germany
[3]Department of Biology, University of Fribourg, Chemin du Musée 10, 1700 Fribourg, Switzerland
[4]Lead Contact
*Correspondence: jan.riemer@uni-koeln.de
https://doi.org/10.1016/j.celrep.2018.12.092

SUMMARY

Disulfide formation in the mitochondrial intermembrane space (IMS) is an essential process. It is catalyzed by the disulfide relay machinery, which couples substrate import and oxidation. The machinery relies on the oxidoreductase and chaperone CHCHD4-Mia40. Here, we report on the driving force for IMS import and on a redox quality control mechanism. We demonstrate that unfolded reduced proteins, upon translocation into the IMS, initiate formation of a metastable disulfide-linked complex with CHCHD4. If this interaction does not result in productive oxidation, then substrates are released to the cytosol and degraded by the proteasome. Based on these data, we propose a redox quality control step at the level of the disulfide-linked intermediate that relies on the vectorial nature of IMS import. Our findings also provide the mechanistic framework to explain failures in import of numerous human disease mutants in CHCHD4 substrates.

INTRODUCTION

In human cells, proteins of the mitochondrial intermembrane space (IMS) fulfil essential functions in calcium signaling, respiratory chain assembly, hypoxia response, and apoptosis signaling. IMS proteins are synthesized by cytosolic ribosomes and are imported into the IMS by dedicated machineries. Many IMS proteins rely not on classical bipartite mitochondrial targeting sequences (MTSs) for their import but, instead, on conserved cysteines that are arranged in specific patterns (Chatzi et al., 2016; Endo et al., 2010; Erdogan and Riemer, 2017; Harbauer et al., 2014; Wasilewski et al., 2017).

These proteins are substrates of the mitochondrial disulfide relay; more specifically, of the IMS import receptor and oxidoreductase CHCHD4 (also human Mia40; in yeast, Mia40) (Banci et al., 2009, 2010; Fischer et al., 2013; Hofmann et al., 2005; Mesecke et al., 2005). CHCHD4 is an unusual oxidoreductase. Unlike oxidoreductases from other oxidizing compartments, like the endoplasmic reticulum or the bacterial periplasm, CHCHD4 does not consist of one or more thioredoxin-like domains but, instead, uses a minimal helix-turn-helix fold containing a hydrophobic groove with chaperone function for substrate interaction (Banci et al., 2009, 2010; Kawano et al., 2009; Koch and Schmid, 2014a). Connected to this fold is a short helix with the redox-active cysteine-proline-cysteine motif (C53 and C55 of human CHCHD4). The N- and C-terminal regions of CHCHD4 are unstructured. At least *in vitro*, they are not required for CHCHD4 function, and a truncated human CHCHD4 can functionally replace Mia40 in yeast cells (Chacinska et al., 2008; Sztolsztener et al., 2013). However, in intact mammalian cells, the N-terminal region serves in the interaction with apoptosis-inducing factor (AIF), which recently has been shown to be critical for the mitochondrial import of CHCHD4 (Hangen et al., 2015; Meyer et al., 2015).

CHCHD4 substrates are synthesized by cytosolic ribosomes as reduced precursors. In the cytosol, members of the glutaredoxin family (in yeast, members of the thioredoxin family) maintain them in their reduced state (Banci et al., 2013; Durigon et al., 2012). Additionally, at least *in vitro*, Zn^{2+} maintains substrates in a reduced state (Morgan et al., 2009). In yeast, the proteasome system fulfils a control function and removes parts of newly produced Mia40 substrates immediately after synthesis (Bragoszewski et al., 2013; Kowalski et al., 2018). It is not known whether this is also the case in mammalian cells.

During passage through the translocase of the outer membrane (TOM) pore, substrates already interact with CHCHD4 (Peleh et al., 2016; von der Malsburg et al., 2011). The initiation of the interaction between CHCHD4 and its substrates therefore depends on two hydrophobic motifs. These motifs are placed in an amphipathic helix that contains a conserved cysteine residue. The first motif consists of hydrophobic residues positioned directly adjacent to this specific substrate cysteine.

In vitro experiments indicated that they initiate a loose non-covalent interaction with the hydrophobic groove of CHCHD4 (Koch and Schmid, 2014b). Subsequently, a hydrophobic patch in the amphipathic helix of the substrate (also termed mitochondrial IMS sorting signal [MISS] or IMS targeting signal [ITS]) that serves as the second motif strengthens this non-covalent interaction (Koch and Schmid, 2014b; Milenkovic et al., 2009; Sideris et al., 2009). Both non-covalent interactions initiate helix folding and orient the substrate and, therefore, allow nucleophilic attack of the thiolate anion of the substrate cysteine residue on CHCHD4. This results in the formation of an intermolecular disulfide bond, likely via C55 of CHCHD4 (Banci et al., 2009; Koch and Schmid, 2014a; Terziyska et al., 2009). This intermolecular disulfide bond is long-lived *in vitro* and *in vivo* compared with intermolecular disulfide bonds that are formed during oxidative protein folding in other compartments (Chacinska et al., 2004; Fischer et al., 2013; Koch and Schmid, 2014a; Mesecke et al., 2005; Petrungaro et al., 2015; Sideris et al., 2009). It has been proposed that this is an adaptation to the coupling of vectorial import and oxidative folding in the IMS that is not found in other oxidizing compartments (Koch and Schmid, 2014a). The intermolecular disulfide is resolved by a second nucleophilic attack from a cysteine of the substrate, which leads to the formation of a disulfide bond in the substrate. The importance of CHCHD4 for substrate import is illustrated by the fact that depletion of CHCHD4 results in loss of its substrates (Fischer et al., 2013; Hangen et al., 2015; Hofmann et al., 2005; Meyer et al., 2015). Likewise, also in yeast, depletion of Mia40 prevents efficient mitochondrial substrate accumulation (Chacinska et al., 2004; Mesecke et al., 2005).

The precise mechanism of vectorial disulfide relay-mediated IMS import remains debated. Initial models based mainly on *in vitro* import experiments in yeast suggested a pathway in which disulfide formation between the substrate and Mia40 leads to directed diffusion of the substrate into the IMS (Milenkovic et al., 2009; Sideris et al., 2009; von der Malsburg et al., 2011). However, these experiments neglected the reducing influences of the cytosol and IMS, the competition of different substrates for import, the chaperone function of Mia40, and the extremely low import efficiency of *in organello* import approaches compared with the highly efficient IMS import in intact cells (Fischer et al., 2013; Kojer et al., 2015). An alternative model proposed that disulfide formation is negligible for protein import and only a consequence of a preceding chaperone-like "pulling" of the substrate by Mia40 that solely relies on hydrophobic interactions (Baker et al., 2012; Peleh et al., 2016; Weckbecker et al., 2012). The latter "*trans*-site receptor" model is based on the fact that the MISS/ITS signal of disulfide relay substrates is both necessary and sufficient for targeting proteins into yeast mitochondria *in vitro*, although, again, the import efficiencies of the respective approaches were very low (Milenkovic et al., 2009; Sideris et al., 2009). Moreover, genetic separation of the oxidoreductase and chaperone function of Mia40 suggested that the oxidoreductase function might not be essential, although the respective experiments were performed in the presence of high amounts of oxidant (Peleh et al., 2016).

The *trans*-site receptor model is contradicted by work in intact cells. Expression of a redox-inactive CHCHD4 mutant (C53S,C55S) in human cells abolished the import and oxidation of selected substrate precursors, although the hydrophobic interaction between the substrate and CHCHD4 was not targeted (Fischer et al., 2013). Additionally, disease mutants like NDUFB10^{C107S} (Friederich et al., 2017) and TIMM8^{C66W} (Hofmann et al., 2002) demonstrated the importance of substrate cysteines because they also fail to accumulate in mitochondria.

To reconcile these apparently exclusive findings and address the important question of how the disulfide relay populates the IMS in intact cells as well as to provide a framework for why disease mutants of CHCHD4 substrates fail to accumulate in the IMS, we revisited the mechanisms of disulfide relay-dependent import in intact mammalian cells. A series of dynamic pulse-chase and proteomic approaches allowed observation of vectorial transport with the correct stoichiometry between the substrate and CHCHD4, the correct spatiotemporal setting of events, in the endogenous redox milieu of the IMS and the cytosol. With our approaches, we demonstrated the formation of a metastable disulfide-linked intermediate between CHCHD4 and the translocating substrate. This intermediate is also formed by substrate variants, including patient mutants, that do not become oxidized and do not accumulate in mitochondria and by CHCHD4 variants that fail to oxidize their substrates. At the level of this intermediate, a decision is made for either productive mitochondrial protein import and oxidation or—if oxidation does not proceed efficiently—substrate release to the cytosol and proteasomal degradation of the unfolded precursor. Thus, the disulfide relay itself provides a layer of quality control for its substrates and determines whether they are competent for folding and import.

RESULTS

In Intact Cells, Cysteine Variants of COX19 Fail to Become Oxidized Despite Formation of Mixed Disulfide Intermediates with CHCHD4

First we explored the spatiotemporal importance of cysteines and hydrophobic interactions in the human disulfide relay by analyzing cysteine mutants in disulfide relay substrates. We therefore mainly focused on selected model twin CX_9C substrate proteins (COX19, COA4, and NDUFB10; Figure S1A). Although IMS proteins that rely on different cysteine motifs for import and oxidative folding have been identified (Barchiesi et al., 2015; Petrungaro et al., 2015; Weckbecker et al., 2012), the majority of known CHCHD4 substrates are members of the twin CX_9C family (Cavallaro, 2010; Fischer et al., 2013; Petrungaro et al., 2015). We generated different HEK293 cell lines that express, in a stable and inducible fashion, hemagglutinin (HA)-tagged substrate variants of COX19, COA4, and NDUFB10. This ensures comparatively low expression levels that lead to full accumulation of wild-type proteins in mitochondria (Fischer et al., 2013). For COX19, we mutated the cysteines that, in the mature protein, form the outer disulfide (C30S,C61S) or the inner disulfide (C40S,C51S). For COA4, we generated a quadruple cysteine mutant to alanine that renders the protein even more hydrophobic, and for NDUFB10, we generated the C107S

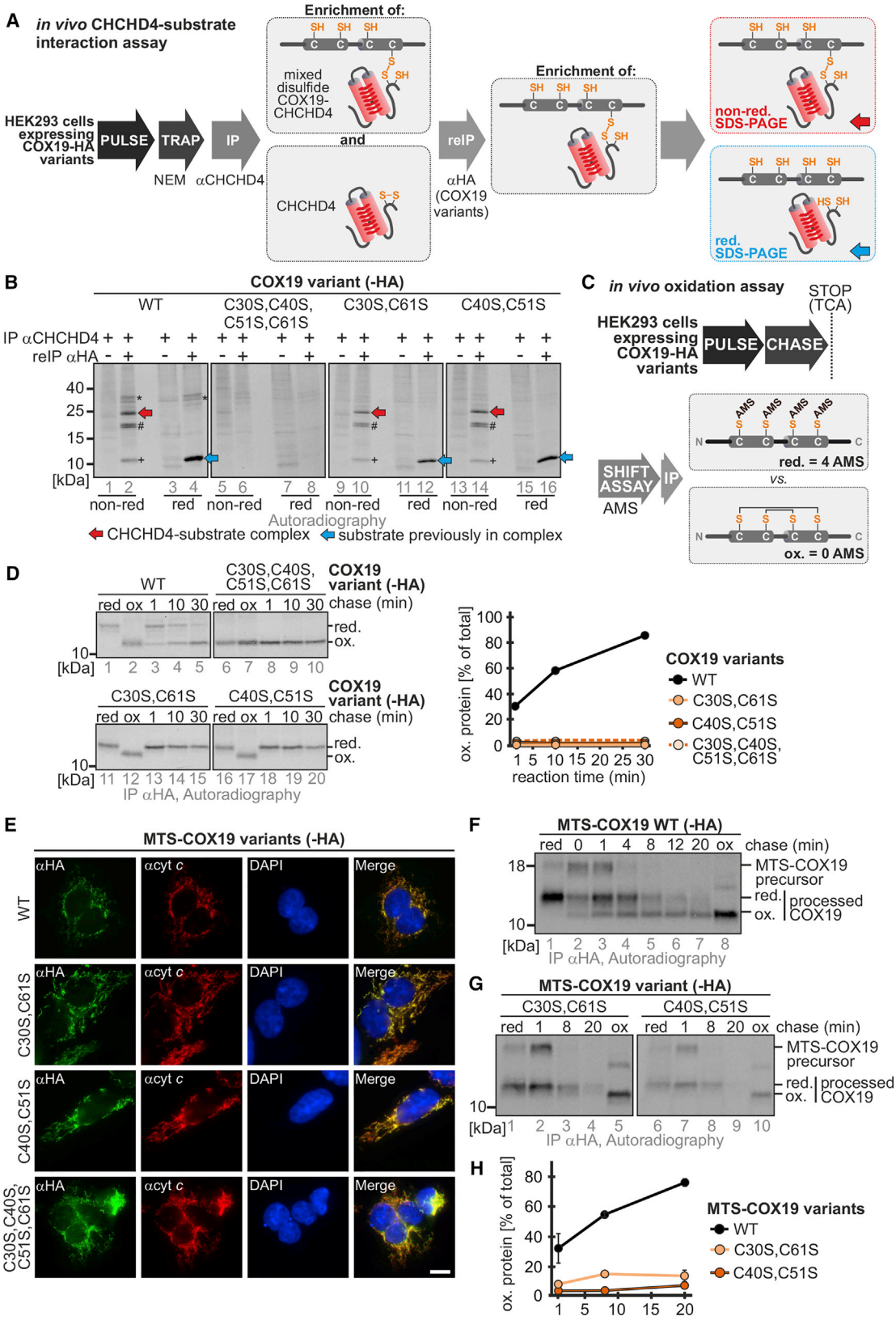

(legend on next page)

mutant, which corresponds to a patient mutation (Friederich et al., 2017; Figure S1A).

Mechanistically, disulfide-linked interaction between CHCHD4 and substrates is the first step in oxidative folding. To test whether COX19 variants form disulfide-linked intermediates with CHCHD4 during their biogenesis in intact cells, we employed a pulse-chase assay followed by denaturing immunoprecipitation (IP) against CHCHD4 and a subsequent denaturing re-IP against the different COX19 variants (Figure 1A). Notably, except for the cysteine-free quadruple mutant of COX19, all variants of COX19 did covalently interact with CHCHD4 (Figure 1B). Wild-type NDUFB10 and the C107S mutant also interacted with CHCHD4 (Figure S1B). Thus, substrates, even when they do not contain the full set of cysteines, traverse the TOM pore and initiate interaction with CHCHD4. It also indicates that not only the cysteine with an adjacent MISS/ITS is capable of interaction with CHCHD4, but, instead, that substrates exhibit a certain plasticity with respect to their CHCHD4 interaction site. In line with this, we found that, for most human twin CX_9C proteins, both helices possess hydrophobic stretches that could serve as alternative CHCHD4 interaction sites (Figure S1C).

Does interaction of substrate cysteine variants with CHCHD4 result in productive oxidation? To test this, we assessed the oxidation kinetics of newly synthesized COX19. To this end, we employed an oxidation assay in which we coupled a pulse-chase assay to redox state determination and IP of the protein of interest (Fischer et al., 2013; Figure 1C). Although wild-type COX19 quickly became oxidized, all cysteine variants remained completely reduced over the course of the experiment (Figure 1D). This is contradictory to *in vitro* experiments in which COX19 cysteine variants did become oxidized by CHCHD4 and also formed mixed disulfide intermediates (Bien et al., 2010; Figures S1D–S1I). Thus, in intact cells, interaction of the substrate and CHCHD4 is not predictive of oxidative folding.

Additionally, we tested whether forced import of COX19 into the IMS by equipping it with an MTS would allow oxidation of COX19 cysteine variants. To this end, we generated stable cell lines expressing $COX19^{C30S,C61S}$, $COX19^{C40S,C51S}$, or $COX19^{C30S,C40S,C51S,C61S}$ fused to the bipartite MTS of the soluble protein SMAC (MTS-COX19 variants). Like MTS-$COX19^{WT}$, all MTS cysteine variants co-localized with mitochondria in immunofluorescence (Figure 1E). As shown previously, oxidation of wild-type COX19 was slightly accelerated when fused to this MTS (Fischer et al., 2013; Figure 1F). However, when we performed the oxidation assay with both MTS cysteine variants, we observed that these proteins did not become oxidized (Figures 1G and 1H). Instead, they appeared to be destabilized (compare with Figure 1D).

Taken together, COX19 cysteine variants, even when efficiently targeted to the IMS, are not oxidized in intact cells. *In vitro*, the proteins still have the capacity to interact with CHCHD4 and become oxidized by it (Figure S1). However, in the *in vivo* situation with its vectorial import and reducing redox milieu, non-productive oxidation is prevented despite an initial covalent interaction between the substrate and CHCHD4 (Fischer et al., 2013; Kojer et al., 2012; Figure 1B).

Interaction with CHCHD4 Does Not Result in Mitochondrial Retention of COX19 Cysteine Variants

Do substrates that interact with CHCHD4 but fail to become oxidized still accumulate in mitochondria? In other words, is the hydrophobic interaction with CHCHD4 sufficient to pull substrates into the IMS? To test this, we analyzed the mitochondrial

Figure 1. Despite Interaction with CHCHD4, COX19 Cysteine Variants Fail to Become Oxidized in Intact Cells

(A) *In vivo* CHCHD4-substrate interaction assay. HEK293 cells stably expressing COX19-HA variants were pulse-labeled with ^{35}S-methionine for 4 h. Then thiol exchange reactions were inhibited by addition of n-ethylmaleimide (NEM) to preserve mixed disulfides. Cells were lysed in SDS, and a denaturing immunoprecipitation (IP) against CHCHD4 enriched monomeric CHCHD4 and mixed disulfides of COX19-HA variants bound to CHCHD4. The latter were isolated by a second IP (re-IP) against the HA tag of COX19-HA variants. This mixed disulfide was analyzed in non-reducing or reducing SDS-PAGE and visualized by autoradiography.

(B) Interaction between CHCHD4 and COX19 cysteine variants, performed as described in (A). 1% of the IP against CHCHD4 was loaded as a control. Expression was induced during the 4-h pulse with 1 μg/mL doxycycline. CHCHD4 interacts covalently with different COX19 cysteine variants *in vivo*. *In silico* analysis suggests that many twin CX_9C substrate proteins contain multiple sites for interaction with CHCHD4 (Figure S1C). Red, reducing SDS-PAGE; non-red, non-reducing SDS-PAGE; red arrow, disulfide-linked CHCHD4-COX19 dimer; blue arrow, COX19; asterisk, background band; #, disulfide-linked CHCHD4-COX19 dimer, possibly with truncated CHCHD4; +, COX19 not in the disulfide-linked complex. n = 2 biological replicates.

(C) *In vivo* oxidation assay to follow oxidative folding in intact cells. Cells are pulse-labeled for 5 min with ^{35}S-methionine and chased with cold methionine for different times. The chase is stopped by trichloroacetic acid (TCA) precipitation, and then the lysate is treated with 4-acetamido-4-maleimidylstilbene-2,2-disulfonic acid (AMS) to determine protein redox states, followed by IP against the HA tag. Eluates are analyzed by Tris-Tricine-PAGE and autoradiography. Reduced COX19 is modified with four AMS, whereas oxidized COX19 remains unmodified.

(D) *In vivo* oxidation assay with HEK293 cells stably expressing different cysteine variants of COX19-HA. COX19 cysteine variants are not oxidized *in vivo*. Performed as described in (C). Expression was induced 1 h before the experiment with 1 μg/mL doxycycline. n = 2 biological replicates.

(E) Localization of MTS-COX19 cysteine variants. COX19 cysteine variants carrying the MTS of SMAC localize to mitochondria. HEK293 cells stably expressing the indicated MTS-COX19-HA variants were incubated for 24 h with 1 μg/mL doxycycline to induce expression. Cells were fixated, permeabilized, and stained using primary antibodies against the HA epitope (αHA, green) and cytochrome *c* (αcyt *c*, red). Nuclei were stained with DAPI (blue). Cells were analyzed by fluorescence microscopy. Scale bar, 10 μm. n = 6–9 cells, 2 biological replicates.

(F) Oxidation kinetics of MTS-COX19-HA wild-type protein. Addition of a cleavable MTS allows oxidation of processed wild-type COX19-HA. Performed as described in (C). n = 2 biological replicates.

(G) Oxidation kinetics of MTS-COX19-HA cysteine variants. Addition of a cleavable MTS does not result in oxidation of COX19 cysteine variants. Performed as described in (C). n = 2 biological replicates.

(H) Quantification of (F) and (G). Quantification was performed in ImageJ.

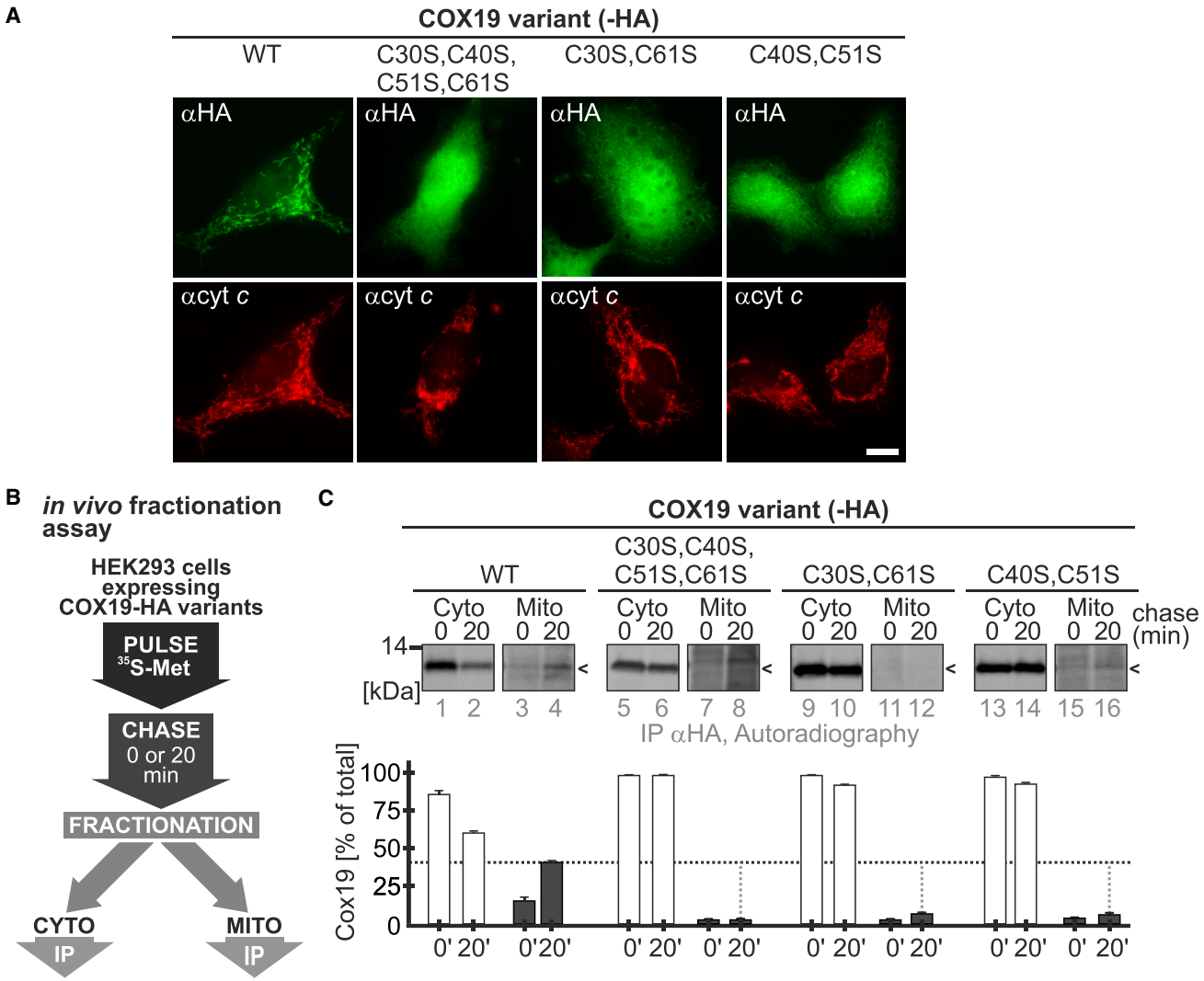

Figure 2. Interaction with CHCHD4 Does Not Result in Mitochondrial Retention of COX19 Cysteine Variants

(A) Immunofluorescence analyses of COX19-HA cysteine variants stably expressed in HEK293 cells. Performed as described in Figure 1E. Although COX19^{WT}-HA accumulates in mitochondria, neither of the cysteine variants does. Instead, they remain in the cytosol. Scale bar, 10 μm. n = 7–10 cells, 2 biological replicates.

(B) *In vivo* fractionation assay to assess post-translational protein import. Expression was induced by doxycycline treatment for 1 h before the pulse-chase experiment. Cells were first pulse-labeled for 5 min with ^{35}S-methionine and then chased with cold methionine for 0 or 20 min. At the end of the chase, cells were transferred to ice and incubated with a low concentration of digitonin for 10 min to selectively permeabilize the plasma membrane and leave the OMM intact. To separate the mitochondrial from the cytosolic fraction, lysates were centrifuged, and COX19-HA variants were immunoprecipitated. Eluates were analyzed by SDS-PAGE and autoradiography.

(C) Pulse-chase fractionation experiment of COX19-HA cysteine variants expressed in HEK293 cells. Although COX19^{WT}-HA accumulates in mitochondria, neither of the cysteine variants does so. Instead, they remain in the cytosol. Performed as described in (B); n = 2 biological replicates.

accumulation of COX19, NDUFB10, and COA4 cysteine variants in stable inducible HEK293 cells. When we tested the cellular localization of these proteins by immunofluorescence, we found that, at steady state, cysteine variants of COX19, NDUFB10, and COA4 failed to co-localize with the mitochondrial marker protein cytochrome *c*. Instead, these variants exhibited cytosolic staining (Figures 2A and S2A; Friederich et al., 2017).

Next we assessed the fate of newly synthesized COX19 and COA4 variants in a dynamic fractionation experiment. With this approach, we coupled a radioactive pulse-chase approach to rapid cell fractionation and IP of the protein of interest (Fischer et al., 2013; Figure 2B). Although wild-type COX19 and COA4 appeared in the mitochondrial fraction after 20 min of chase time, the cysteine variants of both proteins remained in the cytosolic fraction (Figures 2C and S2B). Although the hydrophobic MISS/ITS motif was present in the cysteine variants, and despite their initial interaction with CHCHD4, substrate cysteine mutants failed to accumulate in mitochondria.

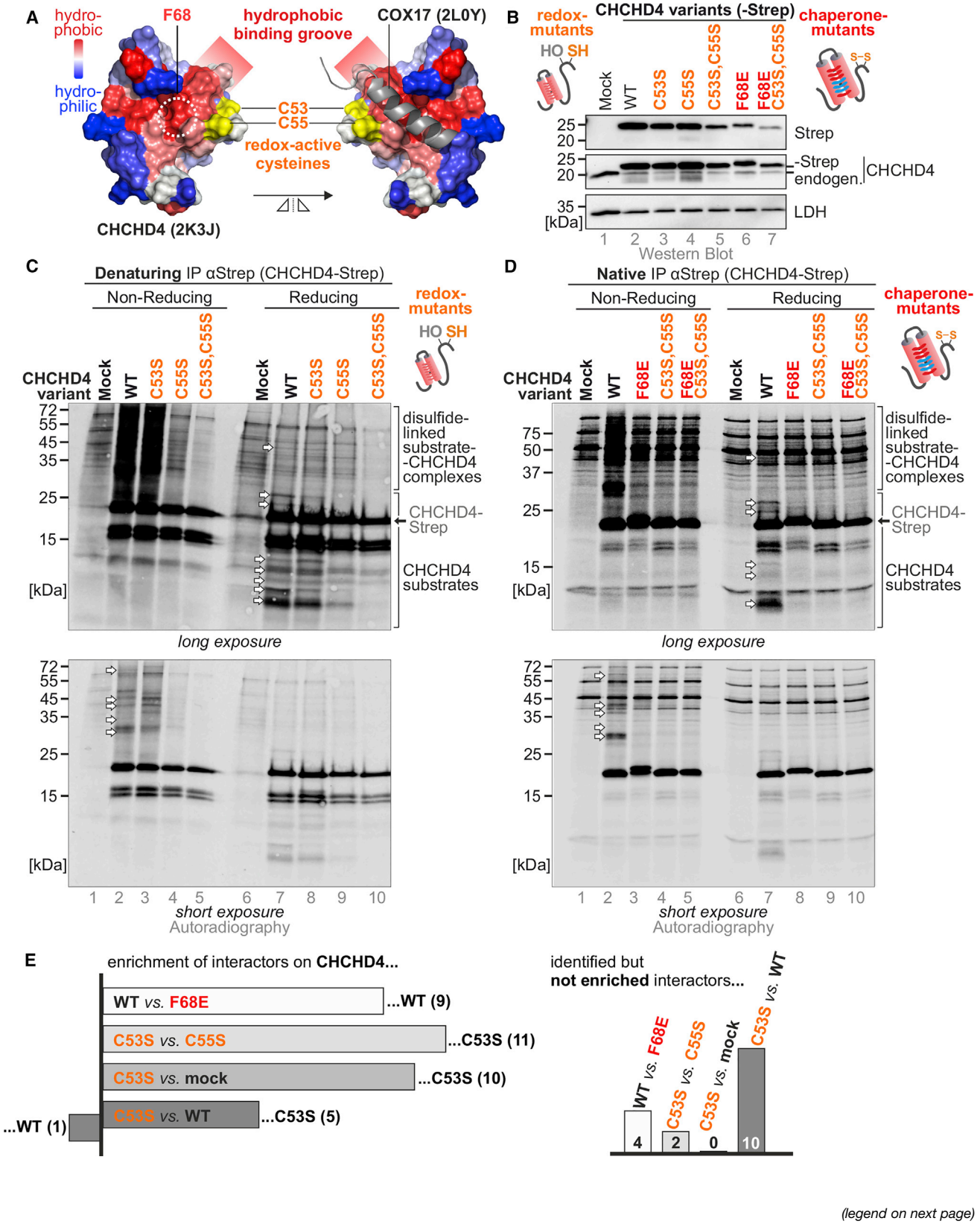

(legend on next page)

Redox-Active Cysteines and the Hydrophobic Groove in CHCHD4 Are Required for Formation of Mixed Disulfide Intermediates with Substrates

The presence of all cysteines is required for efficient oxidation and substrate accumulation in mitochondria. Therefore, it is conceivable that formation of a covalent substrate-CHCHD4 complex also requires the presence of cysteines in CHCHD4. However, recent studies emphasized the importance of the hydrophobic groove in CHCHD4 for substrate import (Banci et al., 2010; Peleh et al., 2016). We thus next dissected "redox" and "chaperone" contributions of CHCHD4 for substrate interaction and oxidation. To this end, we employed HEK293 cell lines stably expressing two sets of C-terminally Strep-tagged CHCHD4 variants. The first set included the "redox-incompetent" variants CHCHD4^{C53S}, CHCHD4^{C55S}, and CHCHD4^{C53S,C55S}. The second set encompassed the chaperone variants CHCHD4^{F68E} and CHCHD4$^{C53S,\ C55S,\ F68E}$ with a mutation in the hydrophobic binding groove of CHCHD4 (Figure 3A). In yeast, different mutations of the hydrophobic binding groove of CHCHD4 have been investigated. The F315E,F318E Mia40 mutant has been shown to be strongly impaired in substrate interaction, oxidation, and import (Kawano et al., 2009; Peleh et al., 2016). However, these mutations change the immediate surroundings of a structural cysteine of Mia40. We deemed it possible that the corresponding mutant might abrogate mitochondrial import of CHCHD4, which, in human cells, depends on its own machinery and the protein AIF and not on the MTS pathway as in yeast (Hangen et al., 2015; Sztolsztener et al., 2013). For our studies, we instead employed the equivalent of the yeast Mia40^{F311E} mutant, CHCHD4^{F68E} (Figure 3A). This mutation is far enough from the structural disulfides in CHCHD4 so that it is not likely to affect CHCHD4 folding. Yeast Mia40^{F311E} also strongly hampered substrate accumulation but impaired viability in Mia40 complementation experiments less severely (Wrobel et al., 2013). All CHCHD4 variants were expressed to similar levels. Exceptions were the F68E-based variants that were present at lower levels, indicating that even this "mild" mutant might be affected in efficient folding (Figure 3B).

With these CHCHD4 variants in hand, we tested the interaction between CHCHD4 and its substrates in radioactive pulse-chase assays, followed by denaturing or native IP of CHCHD4 variants (Figures 3C and 3D). This assay allows testing the transient interaction between CHCHD4 and its substrates that is lost upon folding of proteins (Figure S3A). In denaturing IP with the redox-incompetent variants of CHCHD4, we observed a strong accumulation of proteins on wild-type CHCHD4 (Figure 3C, lanes 2 and 7) compared with mock and CHCHD4^{C53S,C55S}. Likewise, CHCHD4^{C53S} co-precipitated many substrates (Figure 3C, lanes 3 and 8). CHCHD4^{C55S} did so to a much lesser extent (Figure 3C, lanes 4 and 9). This indicates that cysteine residue 55 is likely the more reactive cysteine residue in the redox-active CPC motif of CHCHD4. This is also in line with our finding that, in intact cells, interaction between CHCHD4 and its reoxidizing enzyme ALR (augmenter of liver regeneration) takes place via C55 (Figure S3B). We therefore provide *in vivo* evidence for previous *in vitro* data (Banci et al., 2009, 2011; Koch and Schmid, 2014a).

Next we explored the interactome of the chaperone variants of CHCHD4 in native IP with detergent concentrations we successfully employed before to analyze the interaction of CHCHD4 and substrates (Petrungaro et al., 2015). We found that substrates co-precipitated preferentially with wild-type CHCHD4 and not with the redox-inactive or chaperone mutants (Figure 3D). CHCHD4 variants were precipitated in similar amounts under these conditions. Substrates likely interacted covalently via disulfide bonds as they migrated at higher molecular weight than CHCHD4 under non-reducing conditions but at lower molecular weight after treatment with a reductant (compare Figure 3D, lanes 2 and 7). These data indicate that the hydrophobic groove in CHCHD4 is critical for initiation of disulfide-linked interactions. This is also in line with previous *in vitro* data (Koch and Schmid, 2014b) but somewhat contradictory to an exclusive role of hydrophobic interactions in substrate import.

To further mechanistically dissect the role of chaperone versus redox function, we determined the redox state of CHCHD4^{F68E} using an inverse redox state determination assay (Erdogan et al., 2018; Figure S3C). We found the CPC motif to be overwhelmingly reduced (Figure S3D). This might be explained by the mechanism of CHCHD4 reoxidation. It relies on ALR, which has to interact with the hydrophobic groove in CHCHD4 to perform reoxidation (Banci et al., 2011). Interfering with this interaction might prevent reoxidation and lead to a reduced CPC motif. The presence of a partially reduced CPC motif might also explain at least some of the experimental outcomes with hydrophobic groove mutants of yeast Mia40 in the past that

Figure 3. Redox-Active Cysteines and the Hydrophobic Groove in CHCHD4 Are Required for Formation of Mixed Disulfide Intermediates with Substrates

(A) Structure of CHCHD4 (PDB: 2K3J) and helix 2 of human COX17 (PDB: 2L0Y). Color-coding represents the hydrophobicity of the amino acids according to the Tanford hydrophobicity scale. The substrate is positioned on the hydrophobic groove of CHCHD4, close to the redox-active cysteines C53 and C55. Phenylalanine F68 is localized in the hydrophobic groove. Its mutation should disturb the CHCHD4-substrate interaction.

(B) Steady-state levels of CHCHD4 variants. Cells stably expressing CHCHD4-Strep variants were induced for 24 h with 1 μg/mL doxycycline. Cells were lysed, and lysates were analyzed by SDS-PAGE and immunoblot with the indicated antibodies. n = 4 biological replicates.

(C and D) Pulse-chase analyses of CHCHD4-substrate interactions. HEK293 cells stably expressing CHCHD4-Strep variants were pulse-labeled with ^{35}S-methionine for 4 h. Then thiol exchange reactions were inhibited by addition of NEM to preserve mixed disulfides. Cells were lysed in 2% SDS for denaturing IP (C, n = 2 biological replicates) or in 1% Triton X-100 for native IP (D, n = 1). Then lysates were subjected to IP against Strep, analyzed by non-reducing or reducing SDS-PAGE, and visualized by autoradiography. Disulfide-linked substrate-CHCHD4 complexes and CHCHD4 substrates are indicated. Mainly CHCHD4^{WT} and CHCHD4^{C53S} interact with CHCHD4 substrates. CHCHD4 chaperone mutants fail to enrich substrates.

(E) Summary of quantitative proteomics analysis (see Figures S3E–S3H and Table S1 for detailed data). For substrate accumulation, C55 and the hydrophobic binding groove are required. When comparing the C53S variant and the wild-type, it appears that some substrates are more enriched on C53S, whereas most substrates appear to interact with both proteins to equal extent. The experiment was reproduced with inverted isotope labeling (n = 2 biological replicates).

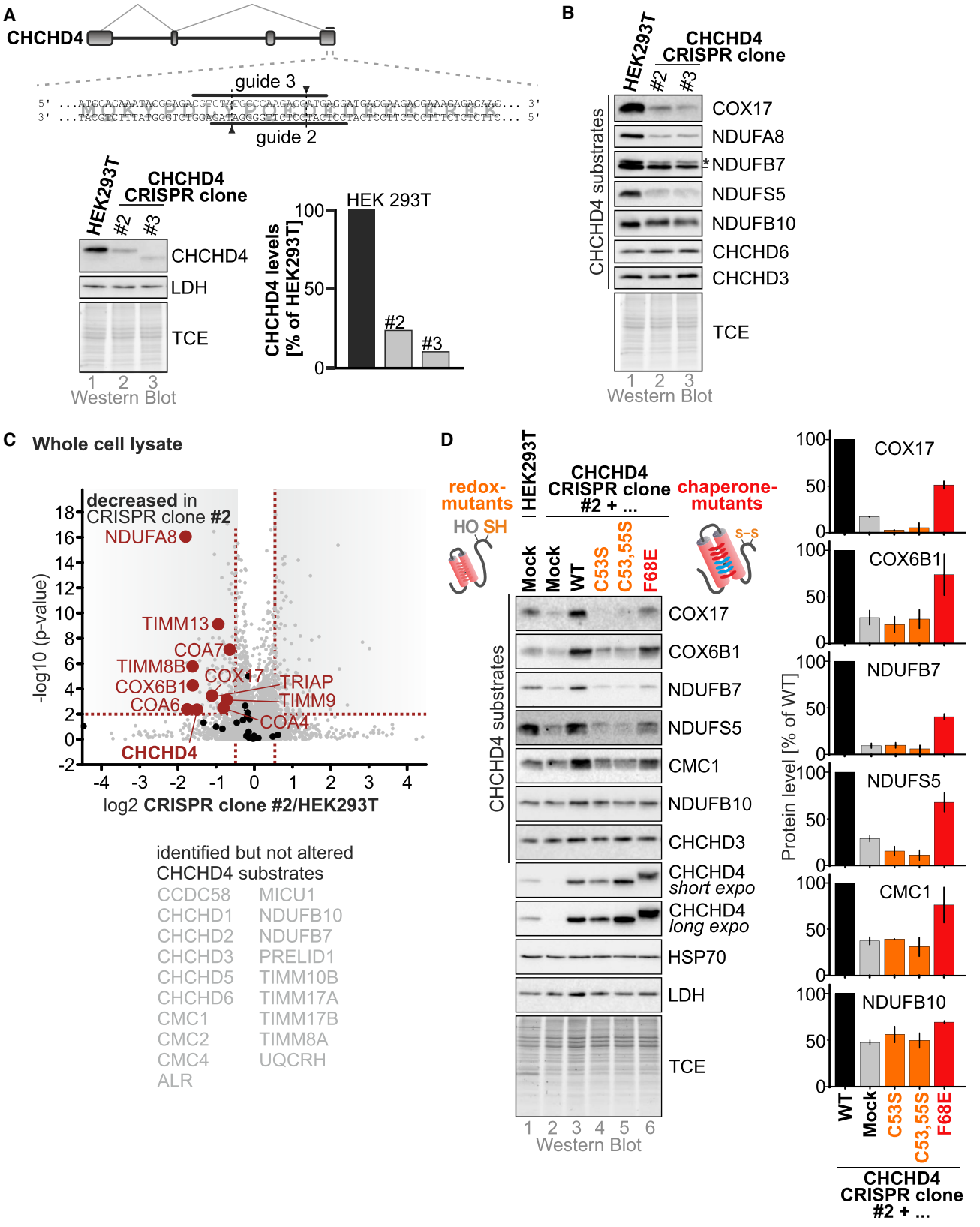

(legend on next page)

emphasized the importance of the hydrophobic groove over the redox-active cysteine motif (Peleh et al., 2016; Wrobel et al., 2013). Thus, both impaired reoxidation by ALR (and thus less oxidized CHCHD4) and decreased substrate interaction appear to underlie the lower efficiency of the CHCHD4^{F68E} variant in the formation of the metastable disulfide-linked CHCHD4-substrate complex.

To specify our analyses, we combined different quantitative proteomics approaches (Figures 3E and S3E–S3H; Table S1). We compared differential accumulation of substrates on CHCHD4 variants. These results supported the findings with pulse-chase assays: cysteine 55 appeared to be most active in substrate interaction (accumulation of substrates on C53S compared with C55S), and the hydrophobic groove in CHCHD4 was required for accumulation of substrates compared with the wild-type (accumulation of substrates on wild-type CHCHD4 compared with the F68E variant). Comparison of CHCHD4^{C53S} and CHCHD4^{WT} indicated that most substrates were not enriched; i.e., both variants bound them to a similar extent. However, some proteins were enriched on CHCHD4^{C53S}. A special case is ALR, which, for CHCHD4 reoxidation, is targeted in a nucleophilic attack by C55. Taken together, these results imply that, in intact human cells, both the redox function and the chaperone function of CHCHD4 are critical for interaction with substrates.

CHCHD4^{F68E} but Not Redox-Inactive CHCHD4 Variants Partially Complement Lack of Endogenous CHCHD4

We next analyzed CHCHD4 redox and chaperone variants in complementation experiments (Figure 4). To this end, we first aimed to generate CHCHD4 knockout cells by employing CRISPR-Cas9 gene editing using guide RNAs targeting different sequences within the CHCHD4 gene. Transfected cells were subsequently sorted, and CHCHD4 expression was examined by western blotting (Figure 4A). Two clonal cell lines (clones #2 and #3) showed a marked reduction in CHCHD4 expression (Figure 4A), and genomic sequence analysis confirmed CRISPR-Cas9-induced insertion or deletion (indel) mutations in CHCHD4. Incomplete ablation of CHCHD4 expression in these cells may rely on an inefficient cell sorting procedure or hemizygous gene mutation in some sorted cells. Independently, reduced CHCHD4 expression in these cells was associated with altered substrate abundance (Figures 4B, 4C, and S4A). Some substrates like COX17 were almost completely lost, whereas others like NDUFB10 were mildly affected. We then complemented the cells with different CHCHD4 variants and tested again for substrate levels as proxy for CHCHD4 function (Figures 4D and S4B). We found that wild-type CHCHD4 complemented loss of CHCHD4. Substrate levels were even slightly increased compared with HEK293T cells (Figure 4D, compare lanes 1 and 3). Conversely, CHCHD4^{C53S} (which we chose because of its strong interaction with substrates) and CHCHD4^{C53S,C55S} could not complement CHCHD4 loss. Instead, it even appeared that expression of CHCHD4^{C53S} further decreased levels of substrates (Figure 4D, compare lanes 2 and 4). Of note, the expression of CHCHD4^{F68E} could at least partially complement the loss of CHCHD4. This indicates that, although in this mutant interaction with substrates was impaired (Figure 3), the capacity for mitochondrial import was still sufficient to partially rescue substrate levels. Collectively, these experiments underline the important role of redox-active cysteines in substrate import.

Mutations of Cysteines in CHCHD4 Are Deleterious for Substrate Oxidation, Import, and Growth

CHCHD4^{C53S} appeared to further decrease substrate levels in the CHCHD4-CRISPR clone. To test whether this mutant exerts a dominant-negative effect, we next investigated oxidation kinetics, substrate levels, and viability in wild-type cells overexpressing CHCHD4 variants. Under these conditions, substrate oxidation kinetics were indeed affected (Figure 5A). Although, for COX19, oxidation was extremely delayed in the presence of all cysteine variants of CHCHD4, the behavior of endogenous NDUFB7 was more graded. Expression of CHCHD4^{C55S} and CHCHD4^{C53S,C55S} delayed NDUFB7 oxidation by about half compared with CHCHD4^{WT}. CHCHD4^{C53S} expression exhibited the strongest delay in oxidation. The differences in oxidation delay caused by CHCHD4 variants indicated that CHCHD4^{C53S} and, to a somewhat lower extent, CHCHD4^{C55S} and CHCHD4^{C53S,C55S} suppress the function of endogenous CHCHD4.

We corroborated and extended our findings with an orthogonal experiment and assessed whether decreased substrate oxidation rates result in lower steady-state substrate levels. Therefore, we expressed different cysteine variants of CHCHD4 in wild-type HEK293 cells for 5 days and tested for levels of diverse substrates. Again, we found that different substrates

Figure 4. The CHCHD4^{F68E} Mutant, but Not CHCHD4 Cysteine Variants, Can Complement Lack of Endogenous CHCHD4

(A) Schematic of the CRISPR-Cas9 strategy to target the CHCHD4 gene. Two guides (#2 and #3) directed against the fourth exon of CHCHD4 (targeting both forms of CHCHD4, CHCHD4.1 and CHCHD4.2) gave rise to clones #2 and #3, respectively. Successful targeting of the gene by both guides was confirmed by sequencing. Use of both guides led to incomplete loss of CHCHD4, as confirmed by immunoblot. n = 3 biological replicates. TCE staining indicates equal loading of proteins.

(A–C) Levels of CHCHD4 substrates in CHCHD4 CRISPR-Cas9 clones. Cell lysates were analyzed by immunoblot against the indicated proteins (B, n = 2 biological replicates) and quantitative mass spectrometry (C, n = 3 biological replicates). Levels of CHCHD4 substrates are differentially affected by depletion of CHCHD4. Many are present at strongly decreased levels. An asterisk indicates the NDUFA8 signal from a preceding decoration of the membrane. TCE staining indicates equal loading of proteins. (A) and (B) are derived from the same experiment and therefore have the same TCE loading control.

(D) Complementation of CHCHD4 CRISPR-Cas9 clones with different CHCHD4 variants. Cell lines were stably transfected with inducible plasmids harboring the indicated variants of CHCHD4 or with the empty vector (Mock). Expression of CHCHD4 variants was induced for 5 days in glucose-containing medium. Cells were lysed, and protein levels were analyzed by SDS-PAGE and immunoblot against the indicated proteins. Expression of wild-type CHCHD4, but not CHCHD4^{C53S} and CHCHD4^{C53S,C55S}, complemented loss of CHCHD4. CHCHD4^{F68E} partially complemented compared with wild-type CHCHD4. Notably, wild-type CHCHD4 overexpression resulted in an increase in levels of selected substrates, and expression of CHCHD4^{C53S} appeared to decrease the levels of some substrates (e.g., COX17 and NDUFS5) even further. n = 2 biological replicates.

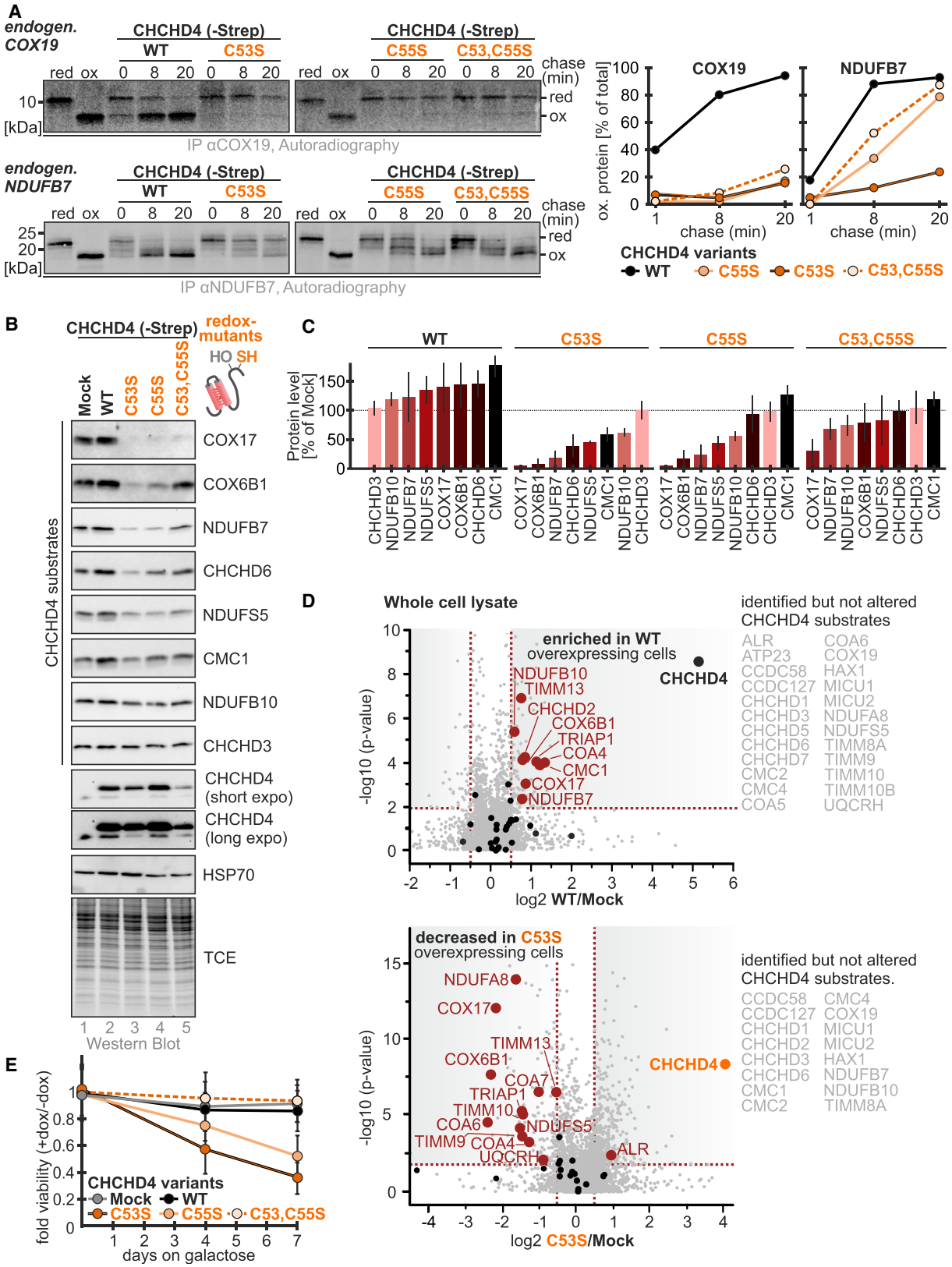

(legend on next page)

were affected to very different degrees by the expression of CHCHD4 variants (Figures 5B and 5C). Although we found that expression of wild-type CHCHD4 generally led to increased steady-state substrate levels compared with the mock control, some substrates, like NDUFB10 and CHCHD3, hardly changed. This supports the notion that, for many substrates, CHCHD4 is normally present in amounts limiting import. Heterogeneity might therefore stem from differences in substrate hydrophobicity, expression levels, and translation and turnover rates. Overexpression of CHCHD4^{C53S,C55S}, but also CHCHD4^{C55S}, resulted in decreased substrate levels for many proteins; some substrates, like COX17, were almost completely depleted. Upon overexpression of CHCHD4^{C53S}, substrate levels were even slightly more decreased (Figures 5B and 5C). Interestingly, expression of the chaperone variant CHCHD4^{F68E} did not result in massively changed substrate levels (i.e., also not increased levels; Figures S5A and S5B). Conversely, expression of CHCHD4$^{C53S,\ C55S,\ F68E}$ showed decreased substrate levels similar to the ones found for expression of CHCHD4^{C53S,C55S}. This also implies that the slightly decreased levels of this variant compared, e.g., with the CHCHD4^{C53S,C55S} variant, do not affect its functional effect (Figure 3B). The findings that redox mutants are deleterious for substrate accumulation and chaperone mutants are not are in line with our observations in the complementation experiments (Figure 4).

To examine the degree of the dominant effect of CHCHD4^{C53S} overexpression in a complimentary unbiased approach, we further employed quantitative proteomics (Figure 5D). Again, CHCHD4^{WT} overexpression resulted in increased levels of multiple substrates, whereas CHCHD4^{C53S} expression reduced substrate levels. Of note, members of the twin CX_3C family of proteins (TIMM9, TIMM10, and TIMM13) were also affected by expression of CHCHD4 variants (Figure 5D).

Expression of CHCHD4 cysteine mutants for 5 days on glucose affected the steady-state levels of its substrates, some of which are subunits or assembly factors of the respiratory chain. Therefore, we tested whether cell growth on galactose, a carbon source requiring respiration, was affected. We induced CHCHD4 variant expression for up to 7 days in cells grown on galactose-containing medium and assessed cell viability using the PrestoBlue assay. We found that overexpression of wild-type CHCHD4 and CHCHD4^{C53S,C55S} did not affect cell growth compared with non-induced cells (Figure 5E). Interestingly, overexpression of the single mutants CHCHD4^{C53S} and CHCHD4^{C55S} led to a strong decrease in cell growth after 7 days compared with non-induced cells. Expression of CHCHD4^{C53S} showed the strongest decrease in growth, mirroring the effect on substrate steady-state levels. Cell growth was not affected upon expression of CHCHD4^{F68E} or CHCHD4$^{C53S,\ C55S,\ F68E}$ (Figure S5C).

Loss of wild-type CHCHD4 oxidoreductase properties resulted in deleterious dominant-negative effects for protein oxidation and cell viability. How could CHCHD4 cysteine mutants suppress the function of endogenous CHCHD4? First, these mutants might displace endogenous CHCHD4 from TOM pores (Fischer et al., 2013), and because they are not capable of substrate oxidation (Figures S5D–S5F), substrates would fail to accumulate in the IMS. However, this does not explain the strong differences between the three mutants (C53S, C55S, and C53S/C55S). The single mutants might still be redox-active and act (especially CHCHD4^{C53S}) as nucleophiles that attack the mixed disulfide bond between endogenous CHCHD4 and the substrate or already partially oxidized substrates. To this end, they had to be in their reduced state. Using the inverse redox state determination assay (Erdogan et al., 2018; Figure S5G), we found that, indeed, both CHCHD4^{C53S} and CHCHD4^{C55S} were completely reduced. We thus propose that both C55 and C53 act as nucleophiles in the mutant backgrounds that attack and destroy the metastable complex of substrate and endogenous CHCHD4 or attack partially oxidized substrates. In both scenarios, disulfide relay efficiency is compromised. This is reflected by slower oxidation rates, lower substrate levels, and decreased respiratory growth. C55 therefore constitutes the more dominant cysteine (also indicated by the strong interaction with substrates of the CHCHD4^{C53S} mutant).

Collectively, based on our results with substrate and CHCHD4 mutants, we propose that substrates can follow two paths from the initially formed metastable covalent substrate-CHCHD4 complex, one leading to productive disulfide formation and another one resulting in the degradation of substrates and, thus, decreased steady-state levels.

Failure of Productive Oxidation Results in IMS Release and Proteasomal Degradation in the Cytosol

If productive substrate oxidation fails to proceed after formation of the mixed disulfide intermediate between substrates and CHCHD4, then substrates are apparently degraded. This is the case for substrate cysteine variants (Figure 1G) but also for substrates in the setting of CHCHD4 cysteine variant expression

Figure 5. CHCHD4 Cysteine Variants that Cannot Oxidize Their Substrates Are Deleterious for Oxidation, Import, and Growth

(A) *In vivo* oxidation assay of endogenous COX19 and NDUFB7 in HEK293 cells stably expressing different cysteine variants of CHCHD4. COX19 and NDUFB7 oxidation is impaired to different extents in the presence of different CHCHD4 cysteine variants. Performed as described in Figure 1C. n = 2 biological replicates.

(B) Steady-state levels of CHCHD4 substrates in HEK293 cells stably expressing different cysteine variants of CHCHD4. Expression of CHCHD4 variants was induced for 5 days in glucose-containing medium. Cells were lysed, and protein levels were analyzed by SDS-PAGE and immunoblot against the indicated proteins. n = 2–3 biological replicates.

(C) Quantification of (B), showing substrate-specific differences in substrate levels.

(D) Steady-state levels of CHCHD4 substrates in HEK293 cells stably expressing wild-type CHCHD4 and CHCHD4^{C53S}. Expression of CHCHD4 was induced for 5 days in glucose-containing medium. Cells lysates were analyzed by quantitative mass spectrometry. In CHCHD4^{WT}-expressing cells, substrate levels were generally increased, whereas in CHCHD4^{C53S}-expressing cells, levels were decreased. n = 3 biological replicates.

(E) Viability of cells upon overexpression of CHCHD4 cysteine variants. CHCHD4^{C53S} and CHCHD4^{C55S} exhibit the most severe effects on cell viability. Expression of CHCHD4 variants was induced for 4 and 7 days in galactose-containing medium. Cells were analyzed by PrestoBlue cell viability reagent. Fold viability is presented as the viability data of induced cells divided by the data of non-induced cells of the same cell line. n = 3 biological replicates.

(Figures 4 and 5). Thus, we next investigated the hypothesis that this degradation takes place in the cytosol (Figure 6). To this end, we first tested whether the proteasome, as the major cytosolic degradation pathway, targets an MTS-COX19 cysteine variant (Figure 6A). MTS-COX19 cysteine variants are processed in the IMS, as indicated by cleavage of its MTS, and then are rapidly degraded (Figures 1G and 6A). Treatment with the proteasomal inhibitor MG132 strongly stabilized the processed form of the MTS-COX19 cysteine variant, which is indicative of release of the processed form from the IMS to the cytosol and subsequent cytosolic degradation. In line with this, MG132-mediated stabilization also resulted in the appearance of cytosolic COX19, further supporting that processed MTS-COX19 is released from the IMS and rapidly degraded in the cytosol (Figures 6B and S6A).

Stabilization upon inhibition of proteasomal degradation also took place for COX19, COA4, and NDUFB10 cysteine variants without MTS (Figures 6C, 6D, and S6B–S6D). This was not the case for the respective wild-type proteins (Figures 6C, 6D, and S6B–S6E), indicating that, in human cells, proteasomal degradation is indeed a mechanism removing proteins that failed the ''test'' for efficient protein oxidation in the IMS.

How could substrate release from the IMS be initiated? In the IMS, reducing enzymes and the highly reducing glutathione pool might contribute to resolving the mixed disulfide bond between the substrate and CHCHD4 (Fischer et al., 2013; Kojer et al., 2012). Although work in yeast has shown that the IMS harbors glutaredoxins and thioredoxins, in the mammalian IMS, only the glutaredoxin GRX1 was found (Pai et al., 2007). If GRX1 influenced disulfide relay import, then its overexpression should be deleterious for substrate accumulation. Indeed, expression of IMS-targeted GRX1 led to decrease of the CHCHD4 substrate COX17 (Figure S6F), the substrate also most affected in assays with the dominant CHCHD4^{C53S}.

It is noteworthy that the degradation pattern appears to be very different for the same COX19 variants with and without MTS (compare Figures 1G and 6A with Figures 1D and 6C). Substrates with an MTS appear to be degraded much faster. Possibly, switching of the import pathway (MTS versus disulfide relay) might explain these more rapid degradation kinetics of the MTS variants. MTS variants are more rapidly imported (Fischer et al., 2013). One might speculate that faster import and, therefore, loss of cytosolic chaperones results in faster IMS release and degradation. By comparison, ''normal'' CHCHD4 substrates might stay longer in the cytosol before entry into the IMS, resulting in increased apparent stability. In our experiments, this would translate into less stable MTS-COX19 variants.

Taken together, substrates that initially enter the IMS and form a complex with CHCHD4 undergo cytosolic degradation when they fail to become efficiently oxidized. This process is likely facilitated by the vectorial nature of IMS protein import. Release of substrates from CHCHD4 would take place at a time when parts of the incoming substrate are still exposed to the cytosol and, thus, could be extracted much more easily.

DISCUSSION

A Redox Quality Control Step in Vectorial Oxidation-Dependent Protein Import into the IMS

Here we present evidence for a redox-dependent ''IMS import quality control step'' (Figure 6E). We propose that the vectorial nature of substrate import and the capacity for productive disulfide formation in combination with the specific redox environment of the IMS form important determinants in this quality control step. This redox quality control is likely embedded in a network of pathways that maintain IMS protein homeostasis, including the unfolded protein response activated by the mistargeting of proteins (UPRam) (Wrobel et al., 2015), mitochondrial precursor overaccumulation stress (mPOS) (Wang and Chen, 2015), mitochondrial compromised protein import response (mito-CPR) (Weidberg and Amon, 2018), and YME1 pathways (Baker et al., 2012; Schreiner et al., 2012).

In our model of the redox-dependent IMS import quality control step, a substrate coming from the cytosol partially traverses the outer mitochondrial membrane (OMM), enters the IMS, and initiates interaction with CHCHD4. Hydrophobic interactions therefore orient the substrate for subsequent formation of the mixed disulfide intermediate between CHCHD4 and its substrate. This intermediate has to persist until further substrate cysteines enter the IMS. We propose that this time span allows the intermediate to serve as a point for decision-making toward either productive disulfide formation or cytosolic substrate degradation. This decision likely depends on the IMS redox environment and IMS redox enzymes like glutaredoxins and thioredoxins (GRX1 is present in the human IMS [Pai et al., 2007, and Trx1 is present in the yeast IMS proteome [Vögtle et al., 2012]). Alternatively, (premature) dissolution of the disulfide in the intermediate might be driven by the second (free) cysteine in CHCHD4 (e.g., C53). This is the reverse reaction of the mixed disulfide bond formation leading to the metastable CHCHD4 substrate intermediate. When the CHCHD4-substrate complex is resolved without productive oxidation, the substrate likely is still in transit across the OMM, allowing it to slide back to the cytosol and undergo degradation. This retrotranslocation probably occurs with the help of cytosolic factors that prevent clogging of TOM pores such as, in yeast, the protein Msp1 (in humans, ATAD1) (Chen et al., 2014; Weidberg and Amon, 2018). Importantly, Msp1/ATAD1 cannot remove substrates from mitochondria that, in the IMS, covalently interact with a folded protein like CHCHD4. Thus, disulfide reduction is a prerequisite for the subsequent removal. The redox-dependent IMS import quality control step therefore avoids accumulation of dead-end CHCHD4 substrate intermediates in the TOM pore and misfolding-prone proteins (e.g., disease mutants lacking individual cysteines) in the IMS. Moreover, such a mechanism would prevent IMS accumulation of (mislocalizing) cytosolic proteins that contain cysteines in a helical context. Thus, the disulfide relay itself provides a layer of quality control for its substrates and determines whether they are competent for folding and import.

With our study, we provide insights into the role of the proteasome in IMS protein import. Previous studies in yeast proposed the degradation of a significant share of proteins before even

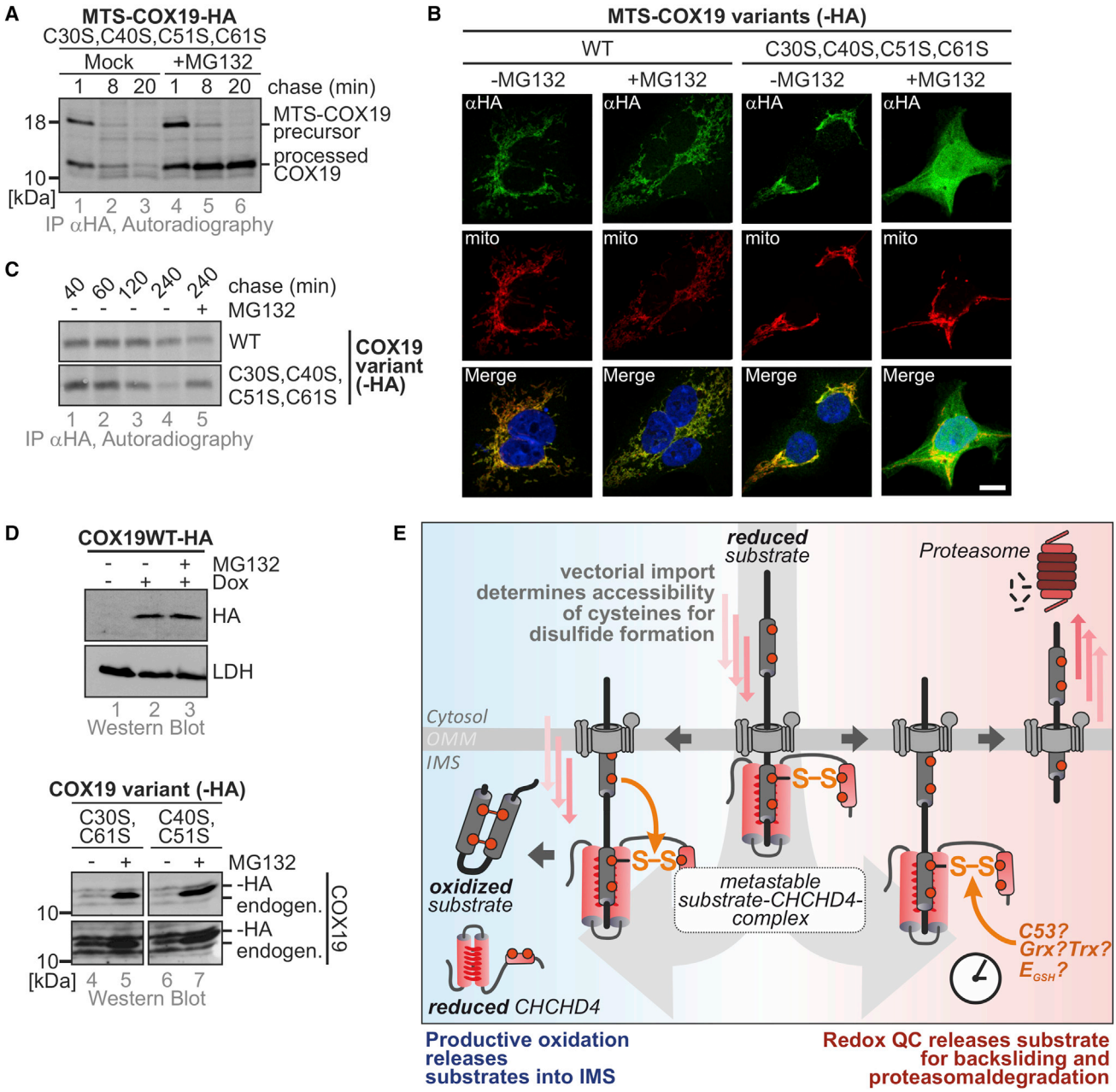

Figure 6. Failure of Productive Oxidation Results in IMS Release and Proteasomal Degradation in the Cytosol

(A) Pulse-chase stability assay of MTS-COX19-C30S,C40S,C51S,C61S-HA in the presence of a proteasomal inhibitor. The destabilized MTS variant C30S,C40S,C51S,C61S is stabilized by MG132 treatment. For proteasome inhibition, 5 μM MG132 was present throughout the pulse-chase experiment. Performed as described in Figure 1C without maleimide modification. Expression was induced 1 h before the experiment with 1 μg/mL doxycycline. n = 2 biological replicates.

(B) Localization of MTS-COX19 cysteine variants in the presence and absence of proteasomal inhibitor. The experiment was performed as described in Figure 1E, except that cells were cultured in the presence or absence of the proteasomal inhibitor MG132 at 5 μM for 4 h. Upon incubation with MG132, the cysteine variant, but not the wild-type of COX19, accumulates in the cytosol. MitoTrackerRed was used to stain mitochondria (mito). Scale bar, 10 μm. WT, n = 35 cells; C30,40,51,61S, n= 10 cells; technical replicates.

(C) Pulse-chase stability assay of COX19 cysteine variants. Cysteine variants, but not the wild-type, are stabilized by MG132 treatment. Performed as described in (A). For proteasome inhibition, 5 μM MG132 was present throughout the pulse-chase experiment. n = 2 biological replicates.

(D) Steady-state levels of COX19 wild-type and cysteine variants. Cysteine variants are stabilized by MG132 treatment. For proteasome inhibition, cells were treated with 5 μM MG132 for 4 h prior to cell lysis. (n = 2 biological replicates)

(E) Model for vectorial protein import by the mitochondrial disulfide relay and the redox quality control step that targets substrates for proteasomal degradation after unsuccessful probing for oxidative folding (see Discussion for details).

reaching the IMS and identified the required E2 and E3 machinery for proteasomal targeting (Ubc4 and Rsp5) (Bragoszewski et al., 2013; Kowalski et al., 2018). In mammalian cells, however, such a massive influence on cytosolic CHCHD4 substrates *en route* to mitochondria appears not to take place (Figures 6C, 6D, and S6B–S6E). Instead, we propose that the proteasome only comes into action after substrates interact with CHCHD4 and fail to be oxidized and imported (Figure 6E). In this scenario, proteasomal degradation is likely also supported by E2 and E3 ligases. These might well be the homologs of Ubc4 and Rsp5 (Kowalski et al., 2018).

Another layer of proteasomal surveillance of the IMS proteome includes reduction and retrotranslocation of mature oxidized proteins followed by their proteasomal degradation (Bragoszewski et al., 2015). This process appeared to take place under very specific conditions. It might well complement the Yme1-dependent control of the mature IMS proteome that has been proposed earlier (Baker et al., 2012; Schreiner et al., 2012), but it is not connected to our proposed IMS import quality control step and would take place at a later time point in the life of a protein.

The Driving Force of CHCHD4-Dependent Import in Intact Cells

Our work also provides insights into the driving force for IMS import by the disulfide relay. Knowledge from structural and *in vitro* experiments points to a mixture of hydrophobic and covalent interactions that initiate oxidative folding. Some models emphasize rapid oxidation of proteins to retain them in the IMS ("folding trap model"). Alternative models focus on the receptor function of CHCHD4. They emphasize non-covalent interactions to drive protein import and suggest that hydrophobic interactions are sufficient for translocation ("*trans*-site receptor model"). In this model, oxidation is a mere consequence of IMS import and not required for the import process (Peleh et al., 2016). However, we think that such models overstress *in vitro* import experiments and neglect the lack of import efficiency observed with these experiments. For example, the import efficiency of cysteine-free Mia40 substrate mutants into yeast mitochondria (Baker et al., 2012; Weckbecker et al., 2012) is usually very low (<10%) compared with the efficient protein import in intact cells. Likewise, import of substrates into yeast mitochondria containing Mia40 only capable of hydrophobic interaction yielded very low import efficiencies (Peleh et al., 2016). Moreover, *in vitro* import assays were performed under oxidizing conditions (i.e., in a buffer under ambient oxygen with redox conditions much more oxidizing than the conditions in the highly reducing cytosol).

Our data, obtained mainly by experiments in intact cells, indicate that hydrophobic interactions alone are, in general, not capable of complementing the lack of disulfide formation. Instead, we propose that, although hydrophobic interactions guide substrate and CHCHD4 toward each other, the covalent interactions in a dynamic metastable complex between CHCHD4 and substrate and the following disulfide formation are the main drivers of efficient protein import in intact cells. This is also in line with the concepts proposed by previous studies (Banci et al., 2009; Sideris et al., 2009; Koch and Schmid, 2014b). Hydrophobic interactions alone might contribute to import of very low amounts of proteins; e.g., proteins that have to be dually localized and that otherwise would become targets of the proposed IMS import quality control step.

Implications for Disease-Causing Substrate Mutants in Human Patients

Our model is also in line with increasing evidence of hampered import of disease mutants of CHCHD4 substrates (e.g., NDUFB10 [Friederich et al., 2017], TIMM8 [Hofmann et al., 2002]), CHCHD10 [Lehmer et al., 2018], and COA6 [Baertling et al., 2015]). Indeed, the patient mutant NDUFB10^{C107S} fails to accumulate in mitochondria despite interacting with CHCHD4 to the same extent as the wild-type protein (Figure S1B). Consequently, we also observed stabilization of this mutant by proteasomal inhibition (Figure S6D). Thus, we propose that the mentioned patient mutants of CHCHD4 substrates fail at the "redox quality control step" presented in this study.

Notably, tissue heterogeneity with respect to mitochondrial accumulation, which we observed, for example, for NDUFB10^{C107S} (Friederich et al., 2017), might indicate differences in the IMS redox milieu, CHCHD4 levels, and redox state and/or quality control and proteasomal activity. This might also point to potential treatment strategies like stimulation of CHCHD4 activity, increase in CHCHD4 levels, suppression of the ubiquitin proteasome system, or rendering the IMS a more oxidizing environment.

STAR★METHODS

Detailed methods are provided in the online version of this paper and include the following:

- KEY RESOURCES TABLE
- CONTACT FOR REAGENT AND RESOURCE SHARING
- EXPERIMENTAL MODEL AND SUBJECT DETAILS
- METHOD DETAILS
  - Pulse Chase Biogenesis assay
  - *In vitro* oxidation kinetics
  - Immunofluorescence
  - Stable Isotope Labeling in Cell Culture and Mass Spectrometric Analysis
  - Assay to address inverse and direct redox states of protein thiols
  - Generation of CHCHD4 CRISPR clones
  - Complementation of CHCHD4 CRISPR clones
  - Western blot analysis for CHCHD4-substrates
  - Quantitative label-free proteomics
  - Viability assay
  - Chemical treatments
  - Structure modeling
  - Hydrophobicity scaling and hierarchical clustering
- QUANTIFICATION AND STATISTICAL ANALYSIS

SUPPLEMENTAL INFORMATION

Supplemental Information includes six figures and two tables and can be found with this article online at https://doi.org/10.1016/j.celrep.2018.12.092.

ACKNOWLEDGMENTS

The Deutsche Forschungsgemeinschaft (DFG; RI2150/1-2, RI2150/2-2, and CRC1218 / TP B02) funds research in the laboratory of J.R. M.H. was a PhD fellow of the Carl Zeiss Stiftung. The CECAD imaging facility provided the microscope setup, and the CECAD proteomics facility supported label-free quantitative proteomics.

AUTHOR CONTRIBUTIONS

J.R. and M.H. designed the study and planned experiments. M.H., S.L.S., L.M.M., M.N.H., M.F., M.A., A.J.E., and C.P. performed experiments and analyzed data. S.A.-E. and J.D. performed the SILAC-based proteomics analysis. H.K. and F.S. helped with generating CRISPR-Cas9 clones. M.H., S.L.S., L.M.M., M.H., and J.R. designed the figures. J.R. and M.H. wrote the manuscript with critical input from C.P. and S.L.S.

DECLARATION OF INTERESTS

The authors declare no competing interests. M.F. is currently employed at Universitätsspital Basel, Switzerland. C.P. is currently employed at ETH Zurich, Switzerland. M.A. is currently employed at PromoCell, Heidelberg, Germany.

Received: August 15, 2018
Revised: November 15, 2018
Accepted: December 20, 2018
Published: January 15, 2019

REFERENCES

Baertling, F., A M van den Brand, M., Hertecant, J.L., Al-Shamsi, A., P van den Heuvel, L., Distelmaier, F., Mayatepek, E., Smeitink, J.A., Nijtmans, L.G., and Rodenburg, R.J. (2015). Mutations in COA6 cause cytochrome c oxidase deficiency and neonatal hypertrophic cardiomyopathy. Hum. Mutat. *36*, 34–38.

Baker, M.J., Mooga, V.P., Guiard, B., Langer, T., Ryan, M.T., and Stojanovski, D. (2012). Impaired folding of the mitochondrial small TIM chaperones induces clearance by the i-AAA protease. J. Mol. Biol. *424*, 227–239.

Banci, L., Bertini, I., Cefaro, C., Ciofi-Baffoni, S., Gallo, A., Martinelli, M., Sideris, D.P., Katrakili, N., and Tokatlidis, K. (2009). MIA40 is an oxidoreductase that catalyzes oxidative protein folding in mitochondria. Nat. Struct. Mol. Biol. *16*, 198–206.

Banci, L., Bertini, I., Cefaro, C., Cenacchi, L., Ciofi-Baffoni, S., Felli, I.C., Gallo, A., Gonnelli, L., Luchinat, E., Sideris, D., and Tokatlidis, K. (2010). Molecular chaperone function of Mia40 triggers consecutive induced folding steps of the substrate in mitochondrial protein import. Proc. Natl. Acad. Sci. USA *107*, 20190–20195.

Banci, L., Bertini, I., Calderone, V., Cefaro, C., Ciofi-Baffoni, S., Gallo, A., Kallergi, E., Lionaki, E., Pozidis, C., and Tokatlidis, K. (2011). Molecular recognition and substrate mimicry drive the electron-transfer process between MIA40 and ALR. Proc. Natl. Acad. Sci. USA *108*, 4811–4816.

Banci, L., Barbieri, L., Bertini, I., Luchinat, E., Secci, E., Zhao, Y., and Aricescu, A.R. (2013). Atomic-resolution monitoring of protein maturation in live human cells by NMR. Nat. Chem. Biol. *9*, 297–299.

Barchiesi, A., Wasilewski, M., Chacinska, A., Tell, G., and Vascotto, C. (2015). Mitochondrial translocation of APE1 relies on the MIA pathway. Nucleic Acids Res. *43*, 5451–5464.

Bien, M., Longen, S., Wagener, N., Chwalla, I., Herrmann, J.M., and Riemer, J. (2010). Mitochondrial disulfide bond formation is driven by intersubunit electron transfer in Erv1 and proofread by glutathione. Mol. Cell *37*, 516–528.

Bragoszewski, P., Gornicka, A., Sztolsztener, M.E., and Chacinska, A. (2013). The ubiquitin-proteasome system regulates mitochondrial intermembrane space proteins. Mol. Cell. Biol. *33*, 2136–2148.

Bragoszewski, P., Wasilewski, M., Sakowska, P., Gornicka, A., Böttinger, L., Qiu, J., Wiedemann, N., and Chacinska, A. (2015). Retro-translocation of mitochondrial intermembrane space proteins. Proc. Natl. Acad. Sci. USA *112*, 7713–7718.

Cavallaro, G. (2010). Genome-wide analysis of eukaryotic twin CX9C proteins. Mol. Biosyst. *6*, 2459–2470.

Chacinska, A., Pfannschmidt, S., Wiedemann, N., Kozjak, V., Sanjuán Szklarz, L.K., Schulze-Specking, A., Truscott, K.N., Guiard, B., Meisinger, C., and Pfanner, N. (2004). Essential role of Mia40 in import and assembly of mitochondrial intermembrane space proteins. EMBO J. *23*, 3735–3746.

Chacinska, A., Guiard, B., Müller, J.M., Schulze-Specking, A., Gabriel, K., Kutik, S., and Pfanner, N. (2008). Mitochondrial biogenesis, switching the sorting pathway of the intermembrane space receptor Mia40. J. Biol. Chem. *283*, 29723–29729.

Chatzi, A., Manganas, P., and Tokatlidis, K. (2016). Oxidative folding in the mitochondrial intermembrane space: A regulated process important for cell physiology and disease. Biochim. Biophys. Acta *1863* (*6 Pt A*), 1298–1306.

Chen, Y.C., Umanah, G.K., Dephoure, N., Andrabi, S.A., Gygi, S.P., Dawson, T.M., Dawson, V.L., and Rutter, J. (2014). Msp1/ATAD1 maintains mitochondrial function by facilitating the degradation of mislocalized tail-anchored proteins. EMBO J. *33*, 1548–1564.

Cox, J., and Mann, M. (2008). MaxQuant enables high peptide identification rates, individualized p.p.b.-range mass accuracies and proteome-wide protein quantification. Nat. Biotechnol. *26*, 1367–1372.

Crooks, G.E., Hon, G., Chandonia, J.M., and Brenner, S.E. (2004). WebLogo: a sequence logo generator. Genome Res. *14*, 1188–1190.

Durigon, R., Wang, Q., Ceh Pavia, E., Grant, C.M., and Lu, H. (2012). Cytosolic thioredoxin system facilitates the import of mitochondrial small Tim proteins. EMBO Rep. *13*, 916–922.

Endo, T., Yamano, K., and Kawano, S. (2010). Structural basis for the disulfide relay system in the mitochondrial intermembrane space. Antioxid. Redox Signal. *13*, 1359–1373.

Erdogan, A.J., and Riemer, J. (2017). Mitochondrial disulfide relay and its substrates: mechanisms in health and disease. Cell Tissue Res. *367*, 59–72.

Erdogan, A.J., Ali, M., Habich, M., Salscheider, S.L., Schu, L., Petrungaro, C., Thomas, L.W., Ashcroft, M., Leichert, L.I., Roma, L.P., and Riemer, J. (2018). The mitochondrial oxidoreductase CHCHD4 is present in a semi-oxidized state in vivo. Redox Biol. *17*, 200–206.

Fischer, M., Horn, S., Belkacemi, A., Kojer, K., Petrungaro, C., Habich, M., Ali, M., Küttner, V., Bien, M., Kauff, F., et al. (2013). Protein import and oxidative folding in the mitochondrial intermembrane space of intact mammalian cells. Mol. Biol. Cell *24*, 2160–2170.

Friederich, M.W., Erdogan, A.J., Coughlin, C.R., 2nd, Elos, M.T., Jiang, H., O'Rourke, C.P., Lovell, M.A., Wartchow, E., Gowan, K., Chatfield, K.C., et al. (2017). Mutations in the accessory subunit NDUFB10 result in isolated complex I deficiency and illustrate the critical role of intermembrane space import for complex I holoenzyme assembly. Hum. Mol. Genet. *26*, 702–716.

Hangen, E., Féraud, O., Lachkar, S., Mou, H., Doti, N., Fimia, G.M., Lam, N.V., Zhu, C., Godin, I., Muller, K., et al. (2015). Interaction between AIF and CHCHD4 Regulates Respiratory Chain Biogenesis. Mol. Cell *58*, 1001–1014.

Harbauer, A.B., Zahedi, R.P., Sickmann, A., Pfanner, N., and Meisinger, C. (2014). The protein import machinery of mitochondria-a regulatory hub in metabolism, stress, and disease. Cell Metab. *19*, 357–372.

Hofmann, S., Rothbauer, U., Mühlenbein, N., Neupert, W., Gerbitz, K.D., Brunner, M., and Bauer, M.F. (2002). The C66W mutation in the deafness dystonia peptide 1 (DDP1) affects the formation of functional DDP1.TIM13 complexes in the mitochondrial intermembrane space. J. Biol. Chem. *277*, 23287–23293.

Hofmann, S., Rothbauer, U., Mühlenbein, N., Baiker, K., Hell, K., and Bauer, M.F. (2005). Functional and mutational characterization of human MIA40 acting during import into the mitochondrial intermembrane space. J. Mol. Biol. *353*, 517–528.

Kawano, S., Yamano, K., Naoé, M., Momose, T., Terao, K., Nishikawa, S., Watanabe, N., and Endo, T. (2009). Structural basis of yeast Tim40/Mia40 as an oxidative translocator in the mitochondrial intermembrane space. Proc. Natl. Acad. Sci. USA *106*, 14403–14407.

Koch, J.R., and Schmid, F.X. (2014a). Mia40 is optimized for function in mitochondrial oxidative protein folding and import. ACS Chem. Biol. *9*, 2049–2057.

Koch, J.R., and Schmid, F.X. (2014b). Mia40 targets cysteines in a hydrophobic environment to direct oxidative protein folding in the mitochondria. Nat. Commun. *5*, 3041.

Kojer, K., Bien, M., Gangel, H., Morgan, B., Dick, T.P., and Riemer, J. (2012). Glutathione redox potential in the mitochondrial intermembrane space is linked to the cytosol and impacts the Mia40 redox state. EMBO J. *31*, 3169–3182.

Kojer, K., Peleh, V., Calabrese, G., Herrmann, J.M., and Riemer, J. (2015). Kinetic control by limiting glutaredoxin amounts enables thiol oxidation in the reducing mitochondrial intermembrane space. Mol. Biol. Cell *26*, 195–204.

Kowalski, L., Bragoszewski, P., Khmelinskii, A., Glow, E., Knop, M., and Chacinska, A. (2018). Determinants of the cytosolic turnover of mitochondrial intermembrane space proteins. BMC Biol. *16*, 66.

Lehmer, C., Schludi, M.H., Ransom, L., Greiling, J., Junghänel, M., Exner, N., Riemenschneider, H., van der Zee, J., Van Broeckhoven, C., Weydt, P., et al. (2018). A novel CHCHD10 mutation implicates a Mia40-dependent mitochondrial import deficit in ALS. EMBO Mol. Med. *10*, e8558.

Mesecke, N., Terziyska, N., Kozany, C., Baumann, F., Neupert, W., Hell, K., and Herrmann, J.M. (2005). A disulfide relay system in the intermembrane space of mitochondria that mediates protein import. Cell *121*, 1059–1069.

Meyer, K., Buettner, S., Ghezzi, D., Zeviani, M., Bano, D., and Nicotera, P. (2015). Loss of apoptosis-inducing factor critically affects MIA40 function. Cell Death Dis. *6*, e1814.

Milenkovic, D., Ramming, T., Müller, J.M., Wenz, L.S., Gebert, N., Schulze-Specking, A., Stojanovski, D., Rospert, S., and Chacinska, A. (2009). Identification of the signal directing Tim9 and Tim10 into the intermembrane space of mitochondria. Mol. Biol. Cell *20*, 2530–2539.

Morgan, B., Ang, S.K., Yan, G., and Lu, H. (2009). Zinc can play chaperone-like and inhibitor roles during import of mitochondrial small Tim proteins. J. Biol. Chem. *284*, 6818–6825.

Pai, H.V., Starke, D.W., Lesnefsky, E.J., Hoppel, C.L., and Mieyal, J.J. (2007). What is the functional significance of the unique location of glutaredoxin 1 (GRx1) in the intermembrane space of mitochondria? Antioxid. Redox Signal. *9*, 2027–2033.

Peleh, V., Cordat, E., and Herrmann, J.M. (2016). Mia40 is a trans-site receptor that drives protein import into the mitochondrial intermembrane space by hydrophobic substrate binding. eLife *5*, e16177.

Petrungaro, C., Zimmermann, K.M., Küttner, V., Fischer, M., Dengjel, J., Bogeski, I., and Riemer, J. (2015). The Ca(2+)-Dependent Release of the Mia40-Induced MICU1-MICU2 Dimer from MCU Regulates Mitochondrial Ca(2+) Uptake. Cell Metab. *22*, 721–733.

Ran, F.A., Hsu, P.D., Wright, J., Agarwala, V., Scott, D.A., and Zhang, F. (2013). Genome engineering using the CRISPR-Cas9 system. Nat. Protoc. *8*, 2281–2308.

Rappsilber, J., Mann, M., and Ishihama, Y. (2007). Protocol for micro-purification, enrichment, pre-fractionation and storage of peptides for proteomics using StageTips. Nat. Protoc. *2*, 1896–1906.

Schindelin, J., Arganda-Carreras, I., Frise, E., Kaynig, V., Longair, M., Pietzsch, T., Preibisch, S., Rueden, C., Saalfeld, S., Schmid, B., et al. (2012). Fiji: an open-source platform for biological-image analysis. Nat. Methods *9*, 676–682.

Schreiner, B., Westerburg, H., Forné, I., Imhof, A., Neupert, W., and Mokranjac, D. (2012). Role of the AAA protease Yme1 in folding of proteins in the intermembrane space of mitochondria. Mol. Biol. Cell *23*, 4335–4346.

Shevchenko, A., Tomas, H., Havlis, J., Olsen, J.V., and Mann, M. (2006). In-gel digestion for mass spectrometric characterization of proteins and proteomes. Nat. Protoc. *1*, 2856–2860.

Sideris, D.P., Petrakis, N., Katrakili, N., Mikropoulou, D., Gallo, A., Ciofi-Baffoni, S., Banci, L., Bertini, I., and Tokatlidis, K. (2009). A novel intermembrane space-targeting signal docks cysteines onto Mia40 during mitochondrial oxidative folding. J. Cell Biol. *187*, 1007–1022.

Suzuki, Y., Ali, M., Fischer, M., and Riemer, J. (2013). Human copper chaperone for superoxide dismutase 1 mediates its own oxidation-dependent import into mitochondria. Nat. Commun. *4*, 2430.

Sztolsztener, M.E., Brewinska, A., Guiard, B., and Chacinska, A. (2013). Disulfide bond formation: sulfhydryl oxidase ALR controls mitochondrial biogenesis of human MIA40. Traffic *14*, 309–320.

Terziyska, N., Grumbt, B., Kozany, C., and Hell, K. (2009). Structural and functional roles of the conserved cysteine residues of the redox-regulated import receptor Mia40 in the intermembrane space of mitochondria. J. Biol. Chem. *284*, 1353–1363.

Tyanova, S., Temu, T., Sinitcyn, P., Carlson, A., Hein, M.Y., Geiger, T., Mann, M., and Cox, J. (2016). The Perseus computational platform for comprehensive analysis of (prote)omics data. Nat. Methods *13*, 731–740.

Vögtle, F.N., Burkhart, J.M., Rao, S., Gerbeth, C., Hinrichs, J., Martinou, J.C., Chacinska, A., Sickmann, A., Zahedi, R.P., and Meisinger, C. (2012). Intermembrane space proteome of yeast mitochondria. Mol. Cell. Proteomics *11*, 1840–1852.

von der Malsburg, K., Müller, J.M., Bohnert, M., Oeljeklaus, S., Kwiatkowska, P., Becker, T., Loniewska-Lwowska, A., Wiese, S., Rao, S., Milenkovic, D., et al. (2011). Dual role of mitofilin in mitochondrial membrane organization and protein biogenesis. Dev. Cell *21*, 694–707.

Wang, X., and Chen, X.J. (2015). A cytosolic network suppressing mitochondria-mediated proteostatic stress and cell death. Nature *524*, 481–484.

Wasilewski, M., Chojnacka, K., and Chacinska, A. (2017). Protein trafficking at the crossroads to mitochondria. Biochim Biophys Acta Mol Cell Res *1864*, 125–137.

Waterhouse, A., Bertoni, M., Bienert, S., Studer, G., Tauriello, G., Gumienny, R., Heer, F.T., de Beer, T.A.P., Rempfer, C., Bordoli, L., et al. (2018). SWISS-MODEL: homology modelling of protein structures and complexes. Nucleic Acids Res. *46* (*W1*), W296–W303.

Weckbecker, D., Longen, S., Riemer, J., and Herrmann, J.M. (2012). Atp23 biogenesis reveals a chaperone-like folding activity of Mia40 in the IMS of mitochondria. EMBO J. *31*, 4348–4358.

Weidberg, H., and Amon, A. (2018). MitoCPR-A surveillance pathway that protects mitochondria in response to protein import stress. Science *360*, eaan4146.

Whitney, P.L., and Tanford, C. (1962). Solubility of amino acids in aqueous urea solutions and its implications for the denaturation of proteins by urea. J. Biol. Chem. *237*, 1735–1737.

Wrobel, L., Trojanowska, A., Sztolsztener, M.E., and Chacinska, A. (2013). Mitochondrial protein import: Mia40 facilitates Tim22 translocation into the inner membrane of mitochondria. Mol. Biol. Cell *24*, 543–554.

Wrobel, L., Topf, U., Bragoszewski, P., Wiese, S., Sztolsztener, M.E., Oeljeklaus, S., Varabyova, A., Lirski, M., Chroscicki, P., Mroczek, S., et al. (2015). Mistargeted mitochondrial proteins activate a proteostatic response in the cytosol. Nature *524*, 485–488.

STAR★METHODS

KEY RESOURCES TABLE

REAGENT or RESOURCE	SOURCE	IDENTIFIER
Antibodies		
Mouse monoclonal anti-Strep	Abcam	Cat# ab184224
Rabbit polyclonal anti-HA	Sigma-Aldrich	Cat# SAB4300603; RRID:AB_10620829
Rat monoclonal anti-HA (used for immunofluorescence)	Roche	Cat#11867423001; RRID:AB_10094468
Mouse monoclonal anti-cytochrome *c*	BD-Biosciences	Cat# 556432; RRID:AB_396416
Mouse monoclonal anti-LDH (H-10)	Santa-Cruz	Cat# sc-133123; RRID:AB_2134964
Rabbit polyclonal anti-COX17	Biorbyt	Cat# orb160552
Rabbit polyclonal anti-COX6B1	Sigma-Aldrich	Cat# HPA004192, RRID:AB_1847180
Rabbit polyclonal anti-NDUFB7	Abcam	Cat# ab188575
Rabbit polyclonal anti-NDUFS5	Abcam	Cat# ab179806
Rabbit polyclonal anti-NDUFA8	Abcam	Cat# ab184952
Rabbit polyclonal anti-CHCHD6	Sigma-Aldrich	Cat# HPA047673; RRID:AB_10961761
Rabbit polyclonal anti-CMC1	Sigma-Aldrich	Cat# HPA043333; RRID:AB_10797139
Rabbit polyclonal anti-NDUFB10	Abcam	Cat# ab196019
Rabbit polyclonal anti-CHCHD3	Abcam	Cat# ab154500
Mouse monoclonal anti-HSP70	Santa-Cruz	Cat# sc-66048; RRID:AB_832518
Mouse monoclonal anti-TIMM8A	Santa-Cruz	Cat# sc-101282; RRID:AB_2204692
Mouse monoclonal anti-TIMM9	Santa-Cruz	Cat# sc-101285; RRID:AB_2287477
Rabbit polyclonal anti-SMAC	Sigma-Aldrich	Cat# SAB3500327; RRID:AB_10638009
Mouse monoclonal anti-PDH	Santa-Cruz	Cat# sc-377092; RRID:AB_2716767
Mouse monoclonal anti-GAPDH	Santa-Cruz	Cat# sc-32233; RRID:AB_627679
Rabbit polyclonal anti-COX19	Fischer et al., 2013, Erdogan et al., 2018	N/A
Rabbit polyclonal anti-ALR	Fischer et al., 2013, Erdogan et al., 2018	N/A
Rabbit polyclonal anti-CHCHD4	Fischer et al., 2013, Erdogan et al., 2018	N/A
Rabbit polyclonal anti-CCS1	Suzuki et al., 2013	N/A
Goat anti-Mouse - Affinity Pure, HRP Conjugate	ImmunoReagents	Cat# GtxMu-003-DHRPX
Goat anti-Rabbit - Affinity Pure, HRP Conjugate	ImmunoReagents	Cat# GtxRb-003-DHRPX
Goat anti-Rat, Alexa Fluor 488	Invitrogen	Cat# A-11006; RRID:AB_2534074
Goat anti-Mouse, Alexa Fluor 594	Invitrogen	Cat# A-31623
Bacterial and Virus Strains		
One Shot TOP10 Chemically Competent *E. coli*	Thermo Fisher	Cat# C404010
Chemicals, Peptides, and Recombinant Proteins		
MG132 (Z-Leu-Leu-Leu-al)	Sigma-Aldrich	Cat #C2211; CAS: 133407-82-6
Critical Commercial Assays		
EasyTag EXPRESS 35S Protein Labeling Mix	Perkin-Elmer	Cat# NEG772
PrestoBlue Cell Viability Reagent	Thermo Fisher	Cat# A13261
TnT Quick Coupled Transcription/Translation System	Promega	Cat# L1170
Pierce 660nm Protein Assay Reagent	Thermo Scientific	Cat# 22660
Deposited Data		
Raw and analyzed MS data – see Table S1	This paper	N/A

(*Continued on next page*)

Continued

REAGENT or RESOURCE	SOURCE	IDENTIFIER
Experimental Models: Cell Lines		
Flp-In T-REx-293-cell lines – see Table S2	Invitrogen	Cat# R78007
Oligonucleotides		
Guide #2 sgRNA2 (antisense) FW: caccgCCTCATCCTCTTGGGGATAG	This paper	N/A
Guide #2 sgRNA2 (antisense) RV: aaacCTATCCCCAAGAGGATGAGGc	This paper	N/A
Guide #3 sgRNA2 (sense) FW: caccgCCTCTATCCCCAAGAGGATG	This paper	N/A
Guide #3 sgRNA2 (sense) RV: aaacCATCCTCTTGGGGATAGAGGc	This paper	N/A
Recombinant DNA		
pSpCas9(BB)-2A-GFP (PX458)s	Addgene, Ran et al., 2013	Cat# 48138
PB-CuO-MCS-IRES-GFP-EF1-CymR-Puro	biocat	Cat# PBQM812A-1
Super PiggyBac Transposase Expression Vector	biocat	Cat# PB210PA-1
Software and Algorithms		
SWISS-MODEL	Waterhouse et al., 2018	https://swissmodel.expasy.org/
Morpheus	Morpheus, https://software.broadinstitute.org/morpheus	https://software.broadinstitute.org/morpheus/
Fiji	Schindelin et al., 2012	https://imagej.net/Fiji
Weblogo	Crooks et al., 2004	https://weblogo.berkeley.edu/

CONTACT FOR REAGENT AND RESOURCE SHARING

Further information and requests for resources and reagents should be directed to and will be fulfilled by the Lead Contact, Jan Riemer (jan.riemer@uni-koeln.de).

EXPERIMENTAL MODEL AND SUBJECT DETAILS

For plasmids and cell lines used in this study, see Table S2. For the generation of stable, inducible cell lines the HEK293 cell line–based Flp-In T-REx-293 cell line was used with the Flp-In T-REx system (Invitrogen). Cells were cultured in DMEM supplemented with 10% fetal bovine serum and penicillin/streptomycin at 37°C under 5% CO_2.

METHOD DETAILS

Pulse Chase Biogenesis assay

Pulse chase assays performed in this study were employed for different experiments. The assay to assess posttranslational import (fractionation assay) and to assess protein oxidation in intact cells (oxidation assay) were performed as described previously (Fischer et al., 2013). Newly synthesized proteins were pulse labeled with EasyTag EXPRESS ^{35}S Protein Labeling Mix (Perkin Elmer) at a concentration of 200 μCi/ml. In oxidation and fractionation assays the pulse labeling was stopped by addition of chase medium containing 20 mM methionine and incubation for indicated times. The chase was stopped by adding ice-cold 8% TCA (oxidation assay) or by addition of 0.003% digitonin to permeabilize selectively the plasma membrane prior to addition of 8% TCA (fractionation assay). After TCA precipitation the samples were resolved in modification buffer and either modified with mmPEG12/24 or left untreated. For interaction assays performed as described in (Petrungaro et al., 2015) no chase medium was added. Instead, thiol exchange reactions were stopped with 15 mM NEM (N-Ethylmaleimide) dissolved in PBS at 4 °C for 15 min. Cells were then lysed in SDS-sample buffer. Prior to immunoprecipitation samples were supplemented with 1% Triton X-100 and cleared by centrifugation at 25,000 × g for 1 h. Immunoprecipitation against protein of interest was carried out at 4°C overnight under gentle shaking. The samples were washed five times before elution with Laemmli buffer (2% SDS, 60 mM Tris, pH 6.8, 10% glycerol, 0.0025% bromphenolblue) for 5 min at 95°C. Samples were analyzed by Tris-Tricine PAGE (oxidation assay) or SDS-PAGE (fractionation assay) and autoradiography.

In vitro oxidation kinetics

The *in vitro* oxidation kinetics assay was performed as described in (Bien et al., 2010). Synthesis of radiolabeled COX19 *in vitro* was performed with the TNT Quick Coupled Transcription/Translation System (Promega). Radiolabeled COX19 was present in its reduced state, as verified by alkylation assays. Prior to incubation with recombinant CHCHD4 variants the radioactive COX19 lysate was diluted 60-fold. The reaction was started by addition of CHCHD4 variants (30 μM final concentration). Samples were TCA-precipitated after indicated times. Pellets were resuspended in modification buffer (0.2 M Tris, pH 7.5, 6 M urea, 10 mM EDTA, 2% SDS) containing 15 mM mmPEG24 before incubation for 1 hr at 25°C. Samples were analyzed by nonreducing SDS-PAGE and autoradiography.

Immunofluorescence

The immunofluorescence assay was performed as described in (Fischer et al., 2013). In short, cells were cultured on poly-L-lysine covered coverslips for 24 hr. Fixation was performed with 4% paraformaldehyde for 15 min. Permeabilization of cell membranes was performed with blocking buffer [20 mM HEPES pH 7.4, 3% BSA, 0.3% Triton X-100] for 1 hr. After washing cells were incubated with primary (anti-HA, anti-Strep, anti-cytochrome *c*) and secondary antibodies (anti-rat, ALEXA488; anti-mouse, ALEXA594) for 1 hr, respectively. Nuclei were stained for 15 min with 2 ng/ml DAPI in PBS. Then, cells were washed, coverslips transferred to microscope slides (cover medium: 30% glycerol, 12% polyvinyl alcohol, 60 mM TRIS, 2.5% 1,4-diazabicyclo-2,2,2-octan) and analyzed by immunofluorescence microscopy. For microscopic images in Figures 1 and 2 the following setup was used: Zeiss Axioskop2, Zeiss Plan-Neofluar 100x/ 1.30/ oil, F-Fiew Cool Snap, CellF imaging software. For microscopic images in Figure 6, S2, and S6 the following setup was used: Leica Microsystems TCS SP8 (Inverse, DMi 8 CS), PL Apo 63x/1.40 Oil CS2, LAS X.

Stable Isotope Labeling in Cell Culture and Mass Spectrometric Analysis

Stable Isotope Labeling in Cell Culture (SILAC) was performed as described in (Petrungaro et al., 2015). The collected beads were heated in SDS-PAGE loading buffer containing 1 mM DTT for 10 min at 95°C. After alkylation using 5.5 mM iodoacetamide for 10 min at room temperature the samples were centrifuged and the supernatants were loaded on 4%–12% gradient gels (NuPAGE, Thermo Fisher) for protein separation. After staining, each gel lane was cut into 5-10 slices, the proteins were in-gel digested with trypsin (Promega) and the resulting peptide mixtures were processed on STAGE tips and analyzed by LC-MS/MS (Rappsilber et al., 2007; Shevchenko et al., 2006). The LC-MS measurements were performed on a QExactive Plus or HF-X mass spectrometer coupled to an EasyLC 1000/1200 nanoflow-HPLC. Peptides were separated on fused silica HPLC-column tip (I.D. 75 μm, New Objective, self-packed with ReproSil-Pur 120 C18-AQ, 1.9 μm (Dr. Maisch) to a length of 20 cm) using a gradient of A (0.1% formic acid in water) and B (0.1% formic acid in 80% acetonitrile in water): loading of sample with 0% B with a flow rate of 600 nl/min; separation ramp from 5%–30% B within 85 min with a flow rate of 250 nl/min).For nanoESI the spray voltage was set to 2.3 kV and ion-transfer tube temperature to 250°C, no sheath and auxiliary gas was used. The mass spectrometer was operated in the data-dependent mode; after each MS scan (mass range m/z = 370 – 1750; resolution: 70000) a maximum of ten MS/MS scans were performed using a normalized collision energy of 25%, a target value of 1000 and a resolution of 17500. The MS raw files were analyzed using MaxQuant Software version 1.4.1.2 (Cox and Mann, 2008) for peak detection, quantification, and peptide identification using a full-length UniProt human database (March, 2016) and common contaminants such as keratins and enzymes used for in-gel digestion as reference. Carbamidomethylcysteine was set as fixed modification and protein amino-terminal acetylation and oxidation of methionine were set as variable modifications. The MS/MS tolerance was set to 20 ppm and three missed cleavages were allowed using trypsin/P as enzyme specificity. Peptide and protein FDR based on a forward-reverse database were set to 0.01, minimum peptide length was set to 7, and minimum number of peptides for identification of proteins was set to one, which must be unique. The "match-between-run" option was used with a time window of 1 min.

Assay to address inverse and direct redox states of protein thiols

The redox state assay was performed as described in (Erdogan et al., 2018). Reduced thiols were blocked by treatment with 15 mM NEM (N-Ethylmaleimide) dissolved in PBS at 4 °C for 15 min for minimal shift (min) and steady-state (ss) samples. Max shift (max) samples were treated with PBS at 4 °C for 15 min. Thiol-exchange reactions were stopped by addition of 8% ice cold TCA. TCA precipitation of proteins was performed by centrifugation at 13,000 × g for 15 min and washing with 5% TCA. Protein precipitates were dissolved in 40 μl of modification buffer by sonication and treated with 5 mM TCEP (Tris(2-carboxyethyl)phosphine) for 15 min at 4 °C before mmPEG24 modification (15 μM final concentration). For min shift controls mmPEG24 was omitted. After modification samples were filled to 100 μl with ddH_2O and Laemmli buffer (2% SDS, 60 mM Tris, pH 6.8, 10% glycerol, 0.0025% bromphenol blue) and 10 μl of sample was loaded and analyzed on SDS-PAGE, western blotting, and immunodetection.

Generation of CHCHD4 CRISPR clones

Guide RNA Sequences (#2: CCTCATCCTCTTGGGGATAG, #3: CCTCTATCCCCAAGAGGATG) targeting human CHCHD4 were cloned into the pSpCas9(BB)-2A-GFP (PX458) vector, which was a gift from Feng Zhang (Addgene plasmid # 48138) (Ran et al., 2013). HEK293T cells were transfected using Lipofectamine 2000 (Thermo Fisher Scientific). After 24 hr, GFP-positive cells were collected via FACS and single cell clones were seeded onto 96-well plates (1 cell / well). Clonal cell lines were screened for CHCHD4 protein expression by western blotting and sequenced to verify indel mutations (by Eurofins GATC Biotech).

Complementation of CHCHD4 CRISPR clones

CHCHD4 CRISPR clones were complemented with different CHCHD4 variants by using the inducible PiggyBac Transposon Vector System. Different CHCHD4 constructs were cloned into the PB-CuO-MCS-IRES-GFP-EF1-CymR-Puro vector and co-transfected with the Super PiggyBac Transposase Expression Vector into the CHCHD4 CRISPR clones by using the transfection reagent FuGene, according to the manufacturer's guideline. After two days, positive clones were selected with 2 μg/ml puromycin in glucose-containing medium.

Western blot analysis for CHCHD4-substrates

HEK293 cells expressing either empty plasmid (Mock) or different CHCHD4-Strep variants, HEK293T CHCHD4 CRISPR clones and HEK293T CHCHD4 CRISPR clones expressing either the empty plasmid (Mock) or different CHCHD4 variants (PiggyBac system) were seeded on 10 cm dishes in glucose-containing medium. After 24 h, the medium was supplemented with doxycycline (Flp-In system) or cumic acid (PiggyBac system) to induce expression of the CHCHD4 variants. No chemical was added to the non-complemented HEK293T CHCHD4 clones. After five days, cells were washed with PBS and lysed in LCW buffer (0.5% Triton X-100, 0.5% sodium deoxycholate, 150 mM NaCl, 20 mM Tris-HCl pH7.5, 10 mM EDTA, 30 mM sodium pyrophosphate, protease inhibitor cocktail (Sigma)). Lysates were incubated for 30 min on ice and cleared by centrifugation at 20.000 x g for 30 min at 4°C. Protein concentration of supernatants was determined with BCA assay (Roth) and 50 μg per lane were analyzed by SDS-PAGE.

Quantitative label-free proteomics

The day before the experiment, cells were seeded on 6-well dishes. The next day, the medium was replaced with DMEM containing 1μg/ml doxycycline induce CHCHD4 variant expression. The cells were incubated for 5 days. After 5 days, medium was removed, cells were washed once with PBS, scratched of in 1 mL PBS and transferred to a 1.5 mL reaction tube. After centrifugation at 500 g for 5 min, PBS was removed and the cell pellets were resuspended in 20 μl lysis buffer (4% SDS in PBS containing protease inhibitor). Then the solution was sonified and incubated for 5 min at 96°C. To precipitate proteins, 160 μl of acetone were added and the samples were frozen at −20°C overnight. After centrifugation for 15 min at 16.000 g, the pellet was washed once with 500 μl acetone and then air-dried. For lin solution digest the pellet was resuspended in 50 μl 8 M Urea in TEAB buffer supplemented with protease inhibitor cocktail. To completely resolve the pellet, samples were sonified. To remove cell debris, samples were centrifuged for 15 min at 20.000 g. The protein concentration of the supernatant was determined using Pierce 660nm Protein Assay Reagent. 50 μg were transferred to a new reaction tube and filled up to 50 μl with the Urea/TEAB buffer. DTT (5 mM end-concentration) was added and the samples were incubated for 1 h at 37°C. Iodoacetamid (40 mM end-concentration) was added and the samples were incubated in the dark for 30 min. Then, Lysyl Endopeptidase with an enzyme to substrate ratio of 1:75 was added, followed by incubation for 4 h at 25°C. Next, the samples were diluted using TEAB buffer to reach a urea concentration below 2 M. Then, trypsin with an enzyme to substrate ratio of 1:75 was added and the samples were incubated at 25°C overnight. To purify the samples, STAGE tips were equilibrated with methanol and buffers containing 0.1% formic acid and 80% acetonitrile. The samples were loaded on the STAGE tips and then washed with the same buffers. After complete drying, the STAGE tips were stored at 4°C until MS analysis, which was performed by proteomics core facility cologne.

All samples were analyzed on a Q Exactive Plus Orbitrap (Thermo Scientific) mass spectrometer that was coupled to an EASY nLC "LC" (Thermo Scientific). Peptides were loaded with solvent A (0.1% formic acid in water) onto an in-house packed analytical column ("50 cm — 75 μm I.D., filled with 2.7 μm Poroshell EC120 C18, Agilent"). Peptides were chromatographically separated at a constant flow rate of 250 nL/min using the following gradient: 3%–5% solvent B (0.1% formic acid in 80% acetonitrile) within 1.0 min, 5%–30% solvent B within 91.0 min, 30%–50% solvent B within 17.0 min, 50%–95% solvent B within 1.0 min, followed by washing and column equilibration. The mass spectrometer was operated in data-independent acquisition mode. The MS1 scan was acquired from 400-1220 m/z at a resolution of 140,000. MSMS scans were acquired for 10 DIA windows at a resolution of 35,000. The AGC target was set to 3e6 charges. The default charge state for the MS2 was set to 4. Stepped normalized collision energy was set to 23.5%, 26%, 28.5%. The MSMS spectra were acquired in profile mode.

Viability assay

The viability of cells in galactose-containing medium (DMEM supplemented with 4.5 g/l galactose, 1 mM sodium pyruvate, 1 x non-essential amino acids, 10% fetal calf serum and 500 μg/ml Pen/Strep) was determined using the PrestoBlue Cell Viability Reagent (Thermo). Galactose adapted HEK293 cells were seeded on 96-well dishes. After 24 h, medium containing doxycycline was added to '+dox-samples' to induce exogenous gene expression. '- dox-samples' were supplemented with medium without doxycycline. Cell viability was assessed either directly after addition of doxycycline (0 days) or after 3 or after 7 days. Each day, the cells were supplemented with fresh medium containing either doxycycline or not. The viability assay was performed according to the manufacturer's protocol. In short, PrestoBlue Cell Viability Reagent was added to the cells in medium. After incubation for 1 h at 37°C, the fluorescence was measured at excitation and emission wavelengths of 560 nm and 590 nm, respectively. After subtracting fluorescence values of medium-only samples the fluorescence values of samples treated with doxycycline were divided by the fluorescence values of samples treated without doxycycline to compare effects of exogenous gene expression.

Chemical treatments

To inhibit the proteasome cells were supplemented with medium containing 5 μM MG132. For western blot analysis, cells were treated for 16 h, while in pulse chase experiments treatment with MG132 started during the starvation period.

Structure modeling

COX19 (Uniprot: Q49B96) and COA4 (Uniprot: Q9NYJ1) were modeled onto the solution structure of the twin CX_9C protein CHCHD7 (PDB: 2LQT) using SWISS-MODEL (Waterhouse et al., 2018). NDUFB10 structure was retrieved from the Cryo-EM structure of human respiratory complex I transmembrane arm (PDB: 5XTC). Structures were visualized with PyMol.

Hydrophobicity scaling and hierarchical clustering

Amino acids in twin CX_9C motifs were scored for hydrophobicity using the Tanford scale (Whitney and Tanford, 1962). Data were grouped using hierarchical clustering (metric: euclidean distance; linkage method: average) and plotted in a heatmap using Morpheus (https://software.broadinstitute.org/morpheus/). Logoplot was created using Weblogo (https://weblogo.berkeley.edu/).

QUANTIFICATION AND STATISTICAL ANALYSIS

Intensity of autoradiography and immunoblot signals were quantified using ImageQuantTL (GE) and Image Lab (Biorad), respectively. Microscope images were processed with Fiji. For SILAC MS data interpretation, Perseus software was used (Tyanova et al., 2016). Interacting proteins were identified by performing outlier tests (Significance A) taking a p value of 0.05, BH corrected, as cut-off. Error bars in figures represent standard deviation. The number of experiments is reported in the figure legend.